Analysis of Atmospheric Factors affecting wildfires

Yujie Li [1,2], Xiaoqing Gao [1,2*], Zhenchao Li [1,2], Junxia Jiang [1,2], Peidu Li [1,2]

[1] Key Laboratory of Land Surface Process and Climate Change in Cold and Arid Regions of Chinese Academy of Sciences, Northwest Institute of Eco-Environment and Resources, Chinese academy of sciences, 320, Donggang West Road, Lanzhou, Gansu, 730000, China

[2] University of Chinese Academy of Sciences, Beijing 100049, China

Abstract

Wildfires have a great impact on the global ecosystem and human society, so the prediction and prevention of wildfires is necessary. This article uses the MOD14A2 data, the NCEP/NCAR and ERA5 Reanalysis data, the GFEDv4 data and the Scripps O_2 data to analyze the correlation between wildfires, meteorological elements and oxygen concentration in the Boreal North America (BONA), the Temperate North America (TENA), the Australia and New Zealand (AUST). The following preliminary conclusions were obtained: 1) From 2001 to 2015, 2002 was the year with the most wildfires, and august was the month with the most wildfires. Besides, Northern Africa, Southern Africa and South America are the main wildfires-affected areas, the total wildfires area from 2001 to 2015 is about 2148 million ha, accounting for nearly 80% of the global wildfires area in these 15 years. 2) Globally, the correlation coefficient between temperature and wildfires area is 0.47, between wind speed and wildfires area is 0.17, between precipitation and wildfires area is -0.41; between relative humidity and wildfires area is -0.19. 3) AS the direct path coefficients of oxygen concentration are nearly 0.38, oxygen can be regarded as a variable independent of meteorological elements. In BONA, from 2001 to 2015, the correlation coefficient between oxygen concentration and wildfires area is 0.61; In TENA, the correlation coefficient is 0.62; In AUST, the correlation coefficient is 0.6. This study illustrates the importance of oxygen concentration for wildfires. So, it is of great significance to the prediction and prevention of global wildfires.

Keywords:

Climate Change; Risk management; Forest; Wildfire; Oxygen concentration

1 Introduction

Forests play a key and dynamic role in the ground and atmospheric systems (Bowman et al., 2009). At the beginning of 21 century, the total area of the world's forests was 3.45 billion ha, accounting for about 25% of the total land area of the earth, and they are unevenly distributed around the world (Li, 2016). Large fires account for a disproportionally high percentage of area burned with potentially severe environmental and socioeconomic impacts (Paulo et al., 2016). The global annual wildfires area from the years 1997 through 2011 varied from 301 to 377 million ha, with an average of 348 million ha (Giglio et al., 2013). Wildfire damage is huge, sudden and strong. It is difficult to dispose of it when it occurs (Shu et al., 2003). Large wildfires may cause soil erosion, soil desertification, the compression of animals, plants and the human living space, at the same time, also cause serious economic losses to the society (Schenk et al., 2002). Annual forest burning produces more than 50% of fossil fuel combustion emissions. Wildfires have caused serious damage to forests, humans, ecosystems and the global environment (IPCC, 2007; Di et al., 2007). Transport of boreal wildfire emissions is a large source of nitrogen oxides over the North Atlantic region (Martin et al., 2008). Wildfires are also about human health. Marlier et al. have shown that (Marlier, 2013) during strong El Niño years, wildfires contribute up to 200 μg m^{-3} and 50 ppb in annual average fine particulate matter ($PM_{2.5}$) and ozone surface concentrations near ignition. The increase of harmful gases seriously endangers human health. Therefore, the prediction and prevention of wildfires is necessary.

Researches based on the spatial and temporal distribution of wildfires and its correlation with meteorological elements are especially important. In recent decades, many scholars have done long-term researches on the relationship between wildfires and meteorological elements. Siegert et al. (2001) suggested that the drought associated with the El Niño/Southern Oscillation (ENSO) destroyed a large area of tropical rainforests around the world, and the drought caused by ENSO caused 2.6 million ha of forest to be burned in 1997-1998. Chen et al. (2017) used satellite data to create a climatology of burned-area and wildfires-emissions responses, drawing on six El Niño and six La Niña events during1997-2016, these observations help to explain why the growth rate of atmospheric CO_2 increases during El Niño and may contribute to improved seasonal wildfires forecasts. Sander et al. (2017) suggested that lightning is one of the main driving forces of large-scale wildfires in North American forests in recent years, affecting the interannual and long-term wildfires and dynamic changes in the burning area of forests in northern North America. It also suggests that lightning ignition increases may increase carbon loss while accelerating the northward expansion of boreal forest. Matt et al. (2014) used the 1979-2013 NCEP data and ECMWF data to calculate three fire risk assessment indices, the US Burning Index (Bradshaw et al., 1983), the Canadian Fire Weather Index (Wagner, 1987), and the Australian (or McArthur) Forest Fire Danger Index (Nobel et al., 1980). The study also shows that a doubling (108.1% increase) of global burnable area is related to meteorological factors such as surface temperature, relative humidity and precipitation. If these meteorological factors are coupled with ignition sources and available fuel, they could markedly impact global ecosystems, societies, economies and climate. Chen et al. (2015) described a climate mode synchronizing forest carbon losses from North and South America by analyzing time series of tropical North Atlantic sea surface temperatures (SSTs), landfall hurricanes and tropical storms, and Amazon wildfires during 1995–2013, found that the relationship between North Atlantic tropical cyclones and southern Amazon wildfires ($r = 0.61$, $p < 0.003$) was stronger than links between SSTs and either cyclones or wildfires alone. Chen et al. (2016) used OCI-burned area relationships and a clustering algorithm, identified 12 hotspot regions in which wildfires had a consistent response to SST patterns.

Furthermore, the scientists also evaluated the importance of oxygen concentration on the fire models. The third series of benchmark experiments (BE3) and the fifth series of benchmark experiments (BE5) of the International Collaborative Fire Model Project (ICFMP) conducted by the Electric Power Research Institute (EPRI) indicate that the oxygen concentration has a very important influence on the error of the fire model (Rowekamp et al., 2008; Lassus et al., 2014).

Although domestic and foreign scholars have made many important researches and contributions to the analysis of wildfires, it has been found that studies of the effect of oxygen concentration on wildfires are seldom. There are many wildfires risk assessment indexes around the world. Most of wildfires risk indexes take into account meteorological elements such as temperature, precipitation, relative humidity, and wind speed, but do not consider the impact of oxygen concentration. Therefore, in order to obtain the influence of oxygen concentration on wildfires, we analyzed the correlation between oxygen concentration and wildfires. Then, further illustrated the importance of oxygen concentration to wildfires. This study can help to better improve the wildfires models and is of great significance to the prediction and prevention of global wildfires.

2 Data and methodology

2.1 Data resource

2.1.1 Global fire data

Global fire data comes from MOD14A2 data (https://modis-land.gsfc.nasa.gov/fire.html). It is a 1km resolution L3 fire mask data product, which synthesized for 8 days. The scientific data set includes fire mask and algorithm quality evaluation. Fire mask is an image filter template used to extract the ignition point. When extracting satellite remote sensing image information, an n*n ground object matrix is used to filter the image elements, and then the required fire point information is displayed. The data we obtained is the number of fire pixels, covering the period from 2001 to 2015.

MOD14A2 data is the accumulated value of each fire pixel category detected by the Terra Moderate-resolution Imaging Spectroradiometer within eight days under the condition of 1km*1km spatial resolution.

2.1.2 Global wildfires area data

Global wildfires area data is derived from GFEDv4 (Global Fire Emissions Database, Version 4.1), provided by NASA (National Aeronautics and Space Administration) (https://daac.ornl.gov/VEGETATION/guides/fire_emissions_v4_R1.html). This dataset provides global estimates of monthly burned area, monthly emissions and fractional contributions of different fire types, daily or 3-hourly fields to scale the monthly emissions to higher temporal resolutions, and data for monthly biosphere fluxes. The study includes 14 areas. The UMD (University of Maryland) land cover type data from GFEDv4 dataset was used to revise the global fires area data, and the coverage period is from 2001 to 2015.

GFED4 burned area data provides global monthly burned area at 0.25*0.25 degree spatial resolution from mid-1995 through the present and daily burned area for the time series extending back to August 2000. The data were derived by combining 500-m MODIS burned area maps with active fire data from the Tropical Rainfall Measuring Mission (TRMM) Visible and Infrared Scanner (VIRS) and the Along-Track Scanning Radiometer (ATSR) family of sensors.

The global fire number data and the global burned area data were corrected by the UMD (University of Maryland) land cover distribution of wildfires in the GFEDv4 data set to obtain the number of wildfires and the wildfires area.

2.1.3 Meteorological data

There are two types of global meteorological data used in this article. One is ERA5 data provided by the European Centre for Medium-Range Weather Forecasts (ECMWF) (https://cds.climate.copernicus.eu/cdsapp#!/dataset/reanalysis-era5-pressure-levels-monthly-means?tab=overview). ERA5 is the fifth-generation ECMWF reanalysis data for the global climate and weather in the past 40 to 70 years. Reanalysis combines observations into globally complete fields using the laws of physics with the method of data assimilation (4D-Var in the case of ERA5). ERA5 provides hourly estimates for a large number of atmospheric, ocean-wave and land-surface quantities. The time period covered is from 2001 to 2015. The use factors include wind speed at 10m, air temperature at 2m, precipitation, relative humidity, and sea level pressure. The spatial resolution of ERA5 reanalysis data is 0.25°x 0.25°.

The second type of data is the NCEP/NCAR reanalysis data set Ⅰ produced by NCEP and NCAR (https://www.esrl.noaa.gov/psd/data/gridded/reanalysis/#opennewwindow). NCEP used the same climate models that were initialized with a wide variety of weather observations: ships, planes, RAOBS, station data, satellite observations and many more. By using the same model, scientists can examine climate/weather statistics and dynamic processes without the complication that model changes can cause.

2.1.4 Observational O_2 concentration data

Observational O_2 concentration data comes from nine stations around the world from the Scripps O_2 program (http://scrippso2.ucsd.edu/). These data come from remote areas or on the ocean, so they represent the average of the large area, not the background information of the station. The nine stations are Alert (Canada), Barrow (Alaska), Cold Bay (Alaska), Cape Kumukahi (Hawaii), La Jolla Pier (California), Mauna Loa Observatory (Hawaii), American Samoa, Cape Grim (Australia), Palmer Station (Antarctica), South Pole. However, the concentration of atmospheric O_2 are reported as changes in the O_2/N_2 ratio of air relative to a reference (air collected in the mid-1980s) to avoid the non-negligible interference caused by dilution effects. The oxygen concentration files contain the average of flask replicates collected at a given station and time, including the standard deviation of the data obtained from flasks. In this paper, the effects of oxygen concentration on wildfires are studied. To avoid errors caused by environmental factors, three sites closer to the forest are selected: Cold Bay, Alaska (BONA); La Jolla Pier, California (TENA); Cape Grim, Australia (AUST).

$$\delta = ((O_2/N_2)_{sample} - (O_2/N_2)_{reference})/(O_2/N_2)_{reference}) \times 10^6 \qquad (2.1)$$

where $(O_2/N_2)_{sample}$ is the O_2/N_2 mole ratio of an air sample and $(O_2/N_2)_{reference}$ is the O_2/N_2 mole ratio of our reference. Our reference is based on tanks of air pumped in the mid-1980s which we store in our laboratory. The unit of δ is per meg.

$$1 \text{ per meg} = 0.20946 \text{ ppm} = \mathrm{M} \times 10^{-6} \times 32\, g/mol\, O_2 = 1.186 \text{ Gt } O_2 \qquad (2.2)$$

where $\mathrm{M} = 3.706 \times 10^{19}\mathrm{mol}$ is a reference value for the total number of O_2 molecules in atmosphere.

Table 1 summarizes the specific information of the data sets used in this study. The wildfires area data and the meteorological data have been normalized.

Table 1 Data Information

elements	data sets	Time resolution	Spatial resolution	unit
Number of fires	MOD14A2 (Thermal Anomalies and Fire 8-Day)	8day	1°x 1°	times
Wind at 10m	NCEP/NCAR Reanalysis Ⅰ ERA5 reanalysis data	hourly and monthly	2.5°x 2.5° 0.25°x 0.25°	m/s
Precipitation	NCEP/NCAR Reanalysis Ⅰ	hourly and	2.5°x 2.5°	mm

	ERA5 reanalysis data	monthly	0.25°x 0.25°	
Temperature at 2m	NCEP/NCAR Reanalysis Ⅰ ERA5 reanalysis data	hourly and monthly	2.5°x 2.5° 0.25°x 0.25°	℃
Relative humidity	NCEP/NCAR Reanalysis Ⅰ ERA5 reanalysis data	hourly and monthly	2.5°x 2.5° 0.25°x 0.25°	%
Surface pressure	ERA5 reanalysis data	monthly	0.25°x 0.25°	hPa
O_2	Scripps O_2 program (O_2/N_2)	monthly	/	$per\ meg$
Wildfires area	GFEDv4	monthly	0.25°x 0.25°	m^2

2.2 Methodology

2.2.1 Method for converting MODIS data into fire point data

Some scholars have suggested that (Ding et al., 2013; Potapov et al., 2008; Stefan et al., 2013) the grayscale attribute of MOD14 data is divided into 0-9. As shown in Table 2, the image grayscale value calculation is mostly used for fire point extraction, so when n>6, N=1, which n for the gray value of fire pixel, and N=1 represents the occurrence of fires. It also indicates that there may be a fire at this place. The number of fires obtained in this paper is the number of fire pixels.

Table 2 MOD14 product data gray value corresponding to fire point

area	**Data and credibility**	
	data	**credibility**
0	No data	/
1 or 2	Unprocessed data	/
3	Water	/
4	Cloud	/
5	Non-fire zone	/
6	Unknown	/
7	Fire point	low confidence
8	Fire point	trusted
9	Fire point	high confidence

2.2.2 Global fire spatial distribution data

Giglio et al. (2006) pointed out that the traditional grid counting number obtained by satellites is biased at high latitudes due to uneven spatial and temporal sampling, so each grid element is observed for multiple satellites and missing observations. The total number of fire pixels is normalized to the original fire pixel count. The corrected fire pixel count of the overpass in the grid cells of row i and column j is expressed as $N'_{fire}(i,j,t)$, Giglio et al. (2006) gave the formula:

$$N'_{fire}(i,j,t) = \frac{N_{fire}(i,j,t)N_{days}(t)A(i)N_{eq}}{N_{total}(i,j,t)A_{eq}} \quad (2.3)$$

where $N_{fire}(i,j,t)$ is number of active fire pixels detected in the grid cell over a given calendar month indexed by t; $N_{total}(i,j,t)$ is the total number of MODIS pixels that fell within the grid cell during the calendar month; $N_{days}(\mathrm{t})$ is the number of days in the calendar month; A(i) is the area of the grid cell (solely a function of i due to the equal-angle grid used to composite pixels); A_{eq} is area of a grid cell along the Equator; N_{eq} is the expected number of MODIS pixels within a grid cell located along the Equator during a full 24-hour day of no missing observations (this value was determined empirically using one year of observations from 2001).

2.2.3 Path analysis

Studies have shown that (Fu et al., 2014; Zhu et al., 2018; Sahanavin et al., 2018; Wu et al., 2015) in order to avoid mistakes in the process of human judgment of the importance of each factor in the analysis process, path analysis of each factor is necessary. This method was originally proposed by the quantitative geneticist Sewall Wright in 1921. The essence is to decompose the correlation coefficient, get the direct effect of a certain independent variable on the dependent variable, the indirect effect and total effect of the dependent variable through other independent variables. r_{ij} is the correlation coefficient of the independent variables X_i and X_j. r_{iY} is the correlation coefficient of X_i and the dependent variable Y, and P_{iY} is the direct path coefficient.

Path analysis starts with a simple correlation coefficient matrix and solves the normalized normal equation of the path coefficient to obtain the direct path coefficient and the inter-turn path coefficient. The principle is as follows:

$$\begin{cases} P_{1Y} + r_{12}P_{2Y} + r_{13}P_{3Y} + \cdots + r_{1k}P_{kY} = r_{1Y} \\ r_{21}P_{1Y} + P_{2Y} + r_{23}P_{3Y} + \cdots + r_{2k}P_{kY} = r_{2Y} \\ r_{31}P_{1Y} + r_{32}P_{2Y} + P_{3Y} + \cdots + r_{3k}P_{kY} = r_{3Y} \\ \cdots\cdots \\ r_{k1}P_{1Y} + r_{k2}P_{2Y} + r_{k3}P_{3Y} + \cdots + P_{kY} = r_{KY} \end{cases} \qquad (2.4)$$

For the normalized normal equations of the above path coefficients,

$$\begin{pmatrix} 1 & r_{12} & r_{13} & \cdots & r_{1k} \\ r_{21} & 1 & r_{23} & \cdots & r_{2k} \\ r_{31} & r_{32} & 1 & \cdots & r_{3k} \\ \vdots & \vdots & \vdots & \cdots & \vdots \\ r_{k1} & r_{k2} & r_{k3} & \cdots & r_{kY} \end{pmatrix} \begin{pmatrix} P_{1Y} \\ P_{2Y} \\ P_{3Y} \\ \vdots \\ P_{kY} \end{pmatrix} = \begin{pmatrix} r_{1Y} \\ r_{2Y} \\ r_{3Y} \\ \vdots \\ r_{kY} \end{pmatrix} \qquad (2.5)$$

Let the coefficient matrix be B, then BP=r. Solve the direct path coefficient $\mathrm{P} = B^{-1}r$. The remaining path coefficient $p_{ye} = \sqrt{1 - p_{1y}r_{1y} - p_{2y}r_{2y} - \cdots - p_{ky}r_{ky}}$.

Path analysis decomposes the simple correlation coefficient into direct path coefficients and inter-turn path coefficients, which is more accurate than correlation analysis and regression analysis, and provides a basis for in-depth study of the causal relationship between the causal variable and the outcome variable through the surface phenomena.

3 Results

3.1 The temporal and spatial changes of global wildfires

3.1.1 The interannual variation of the number of global wildfires

According to Fig.1, the year of frequent wildfires was in 2002, with 213,041 wildfires occurring worldwide in one year; followed by 2012, with 209,021 wildfires occurring worldwide in a year. The year with the least number of wildfires occurred in 2013, with 187,436 wildfires occurring worldwide in a year, followed by 2009, with 190,976 wildfires worldwide. In the 15 years from 2001 to 2015, there were a total of 3000,364 wildfires worldwide, with an average of 200,024 wildfires per year. The most frequent month of global wildfires is August, the total number of global wildfires can reach 327,083 times; the second is October, the total number of wildfires can reach 324,897; the least months are January, February and December. Among them, the number of global wildfires occurred in January was the lowest in 12 months, with 165,523 times, accounting for only 50.6% of the most wildfires in August (Fig.2). In the years when there are the most global wildfires, such as 2002 and 2012, there are more wildfires in the corresponding months. The most frequent occurrences of wildfires such as 2, 4, 5, 6, 7, 8, 9, and 11 are in one of 2002 and 2012. In the years when there are fewer global wildfires, such as 2009 and 2013, the number of wildfires in each month is relatively small.

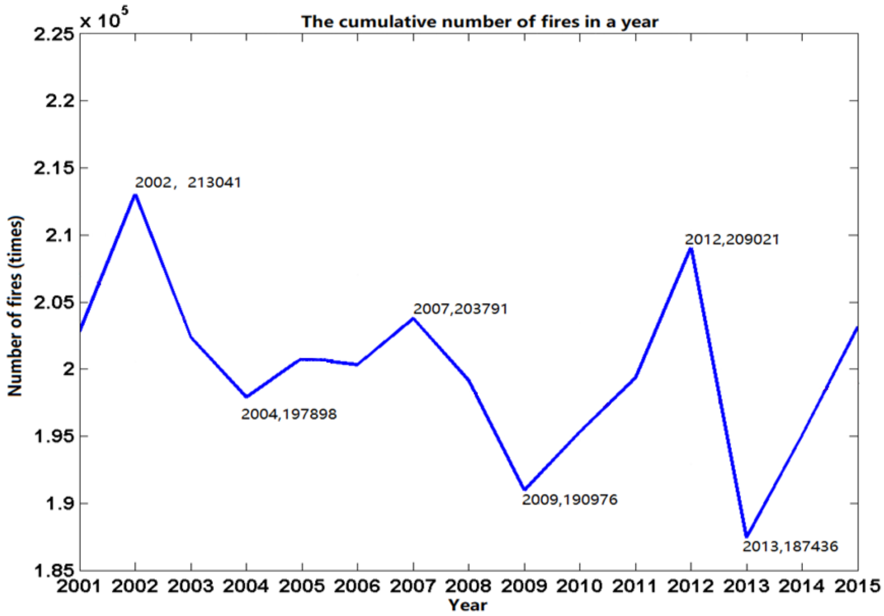

Fig.1 Interannual variations of the number of global wildfires from 2001 to 2015.

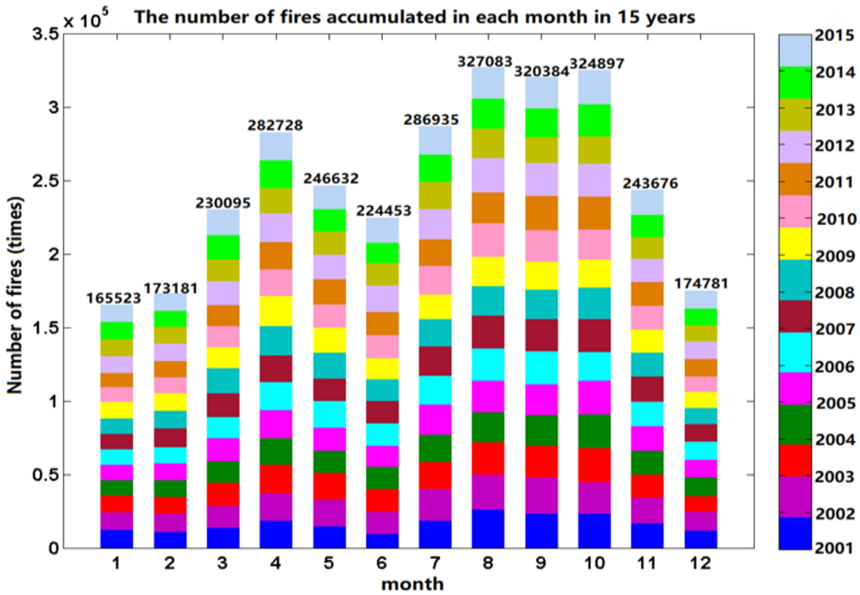

Fig.2 Statistics on the cumulative number of wildfires in each month in the 15 years from 2001 to 2015, Different colors represent different years

3.1.2 Spatial distribution characteristics of wildfires

From the distribution of the world forest resources in Fig.3 (http://www.fao.org/home/zh/), it can be seen that the global forests are mainly distributed in central Africa, the Amazon basin in South America, the northern North America, the Asia-Pacific region, the Central and Western Europe regions. The South American Amazon Basin is the world's most extensive tropical rainforest region, accounting for half of the tropical rain forest area and 20% of the global forest area, and has an important regulatory role for climate and ecology.

According to formula (2.3), the spatial distribution of global fire numbers can be obtained. Fig.4 shows the spatial distribution of global fires from 2001 to 2015. Compare Fig.3 with Fig.4, we find that the distribution of global wildfires has obvious spatial distribution characteristics: wildfires in North America are mainly distributed in Mexico, Canada, and the eastern United States, and there are fewer wildfires in Alaska; wildfires in South America are mainly distributed in Brazil in the Amazon basin; wildfires in Africa are mainly distributed in western Africa, southern Africa, parts of eastern Africa and central regions, and wildfires in the Congo Basin are particularly serious; European wildfires are mainly distributed in Western European countries and Russia; Asian wildfires are mainly distributed in Eastern Siberia alpine region and China; Oceania wildfires are mainly distributed in coastal areas, deserts are mainly in the central and southwestern parts of Australia. Among them, the more serious wildfires are Central Africa, Southern Africa and the Amazon Basin.

Summarize the distribution and changes of global wildfires in the past 15 years: Brazil's forests in South America, central and southern Africa have serious disasters; there were no obvious observable wildfires in Alaska and Canada only in 2001, 2006, 2008, and 2014; in the eastern part of Russia in the Eurasian region, there were no obvious observable wildfires in 2004, 2006 and 2011; in the Australian forest covered in Oceania, the wildfire disasters slowed significantly in 2003, 2004, 2005, 2008, 2010 and 2013; the wildfires in Africa and South America were the most serious in 2002 and 2012. The wildfire disasters slowed down in 2004, 2009 and 2013, which is consistent with the cumulative results of the number of global wildfires in the year, indicating that the central and southern regions of Africa and the Amazon basin in South America are The region with the most serious wildfires in the world is also the region with the largest ‘contribution’ of accumulated wildfires in a year.

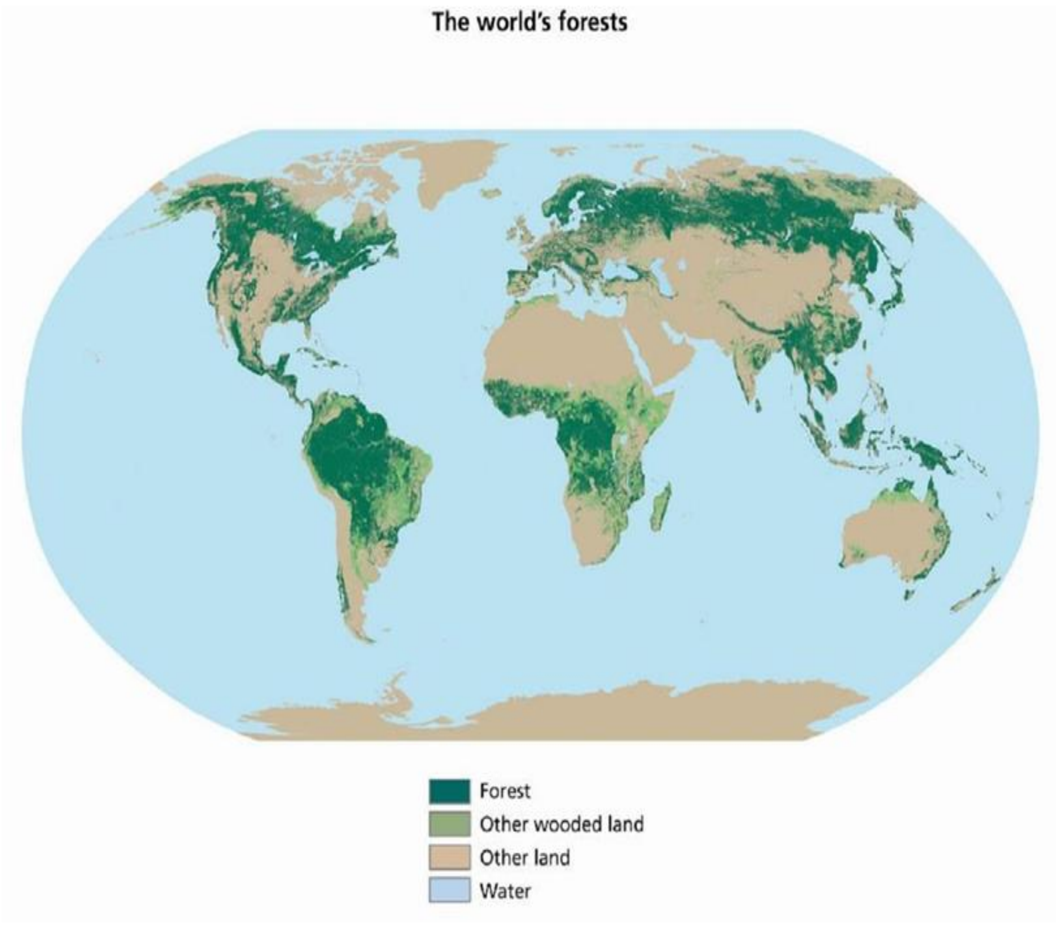

Fig.3 The distribution of the world's forests

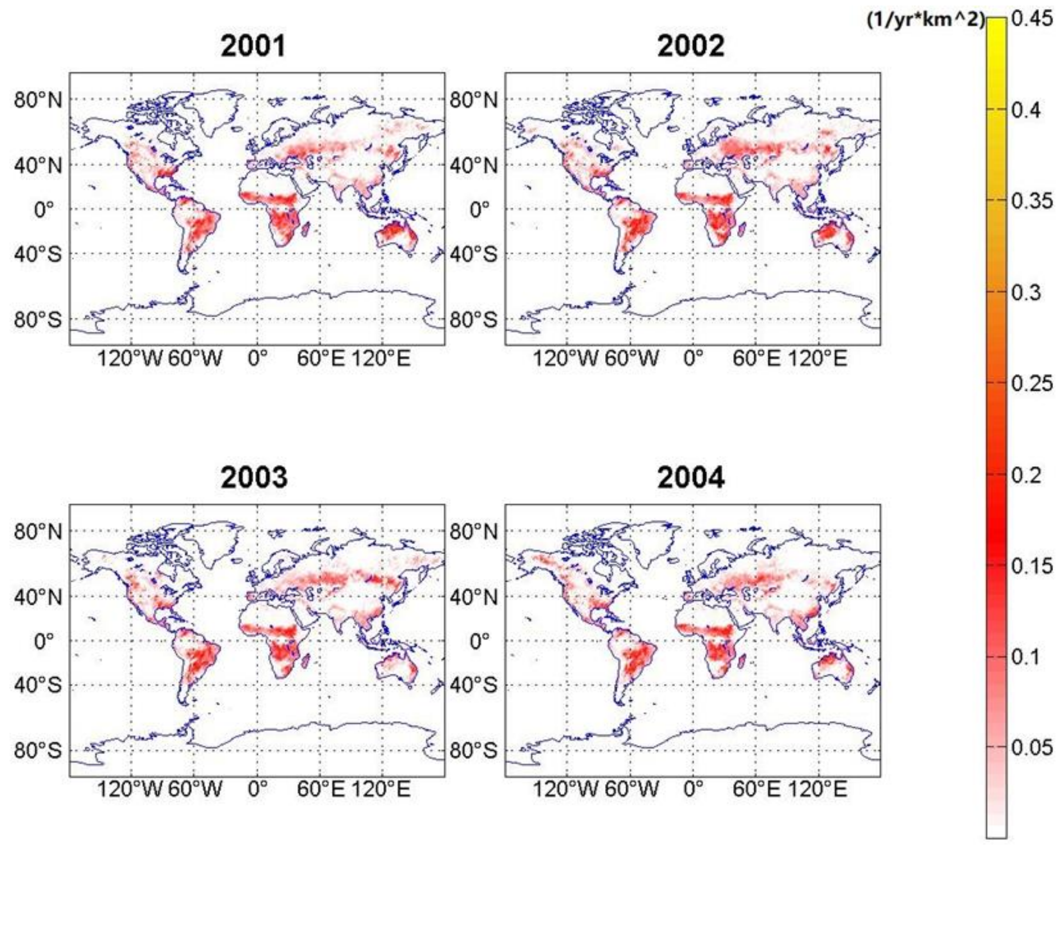

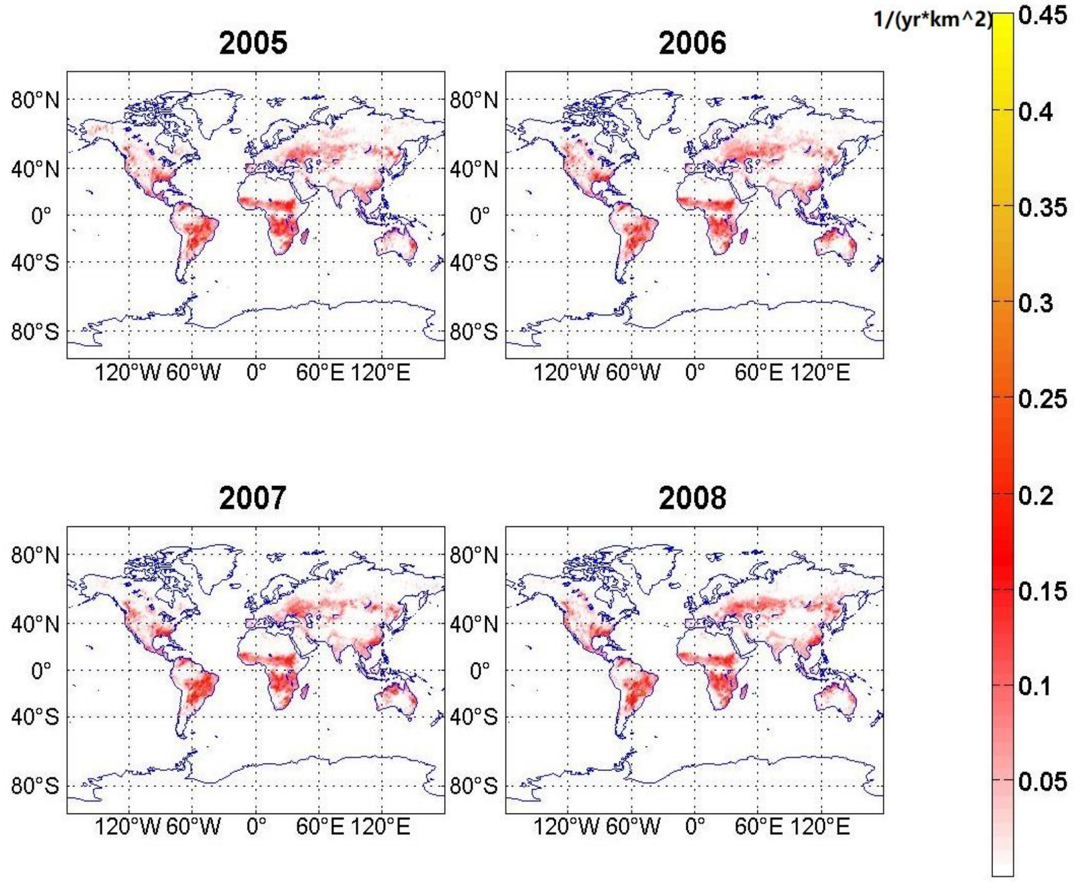
2005
2006
2007
2008
80°N
40°N
0°
40°S
80°S
120°W 60°W 0° 60°E 120°E
1/(yr*km^2)
0.45
0.4
0.35
0.3
0.25
0.2
0.15
0.1
0.05

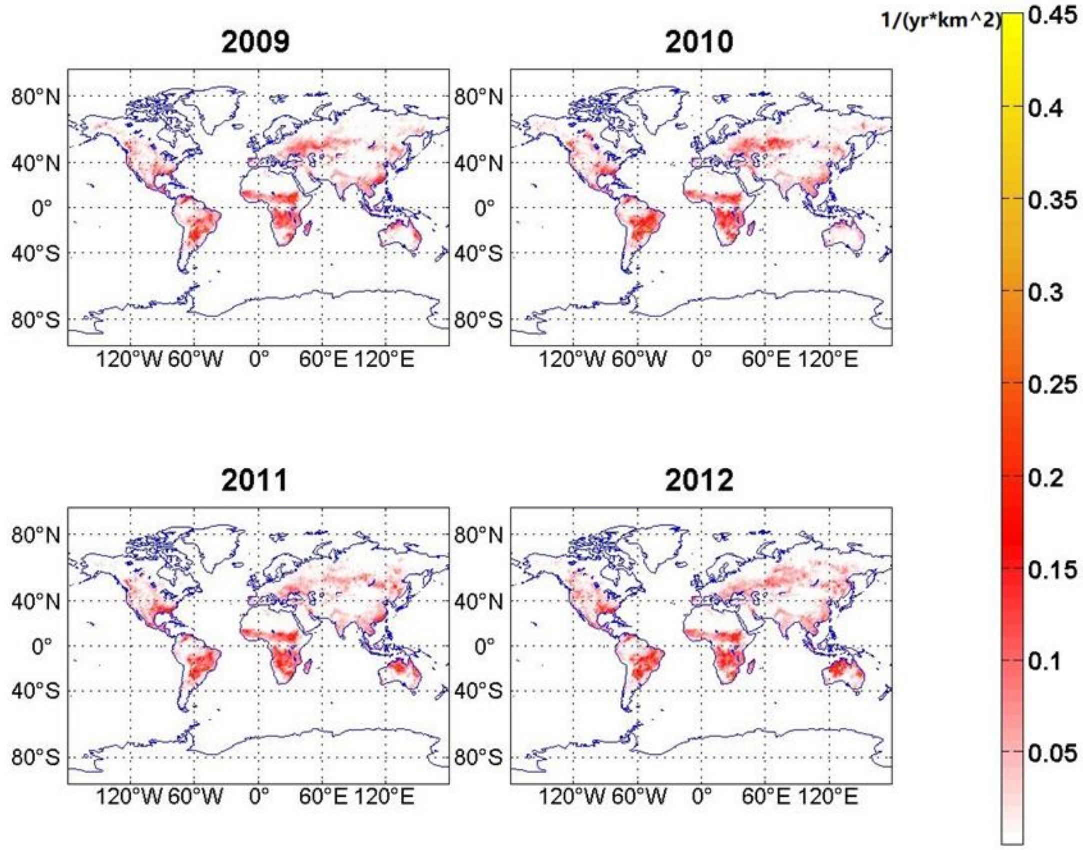
2009
2010
2011
2012
80°N
40°N
0°
40°S
80°S
120°W 60°W 0° 60°E 120°E
1/(yr*km^2)
0.45
0.4
0.35
0.3
0.25
0.2
0.15
0.1
0.05

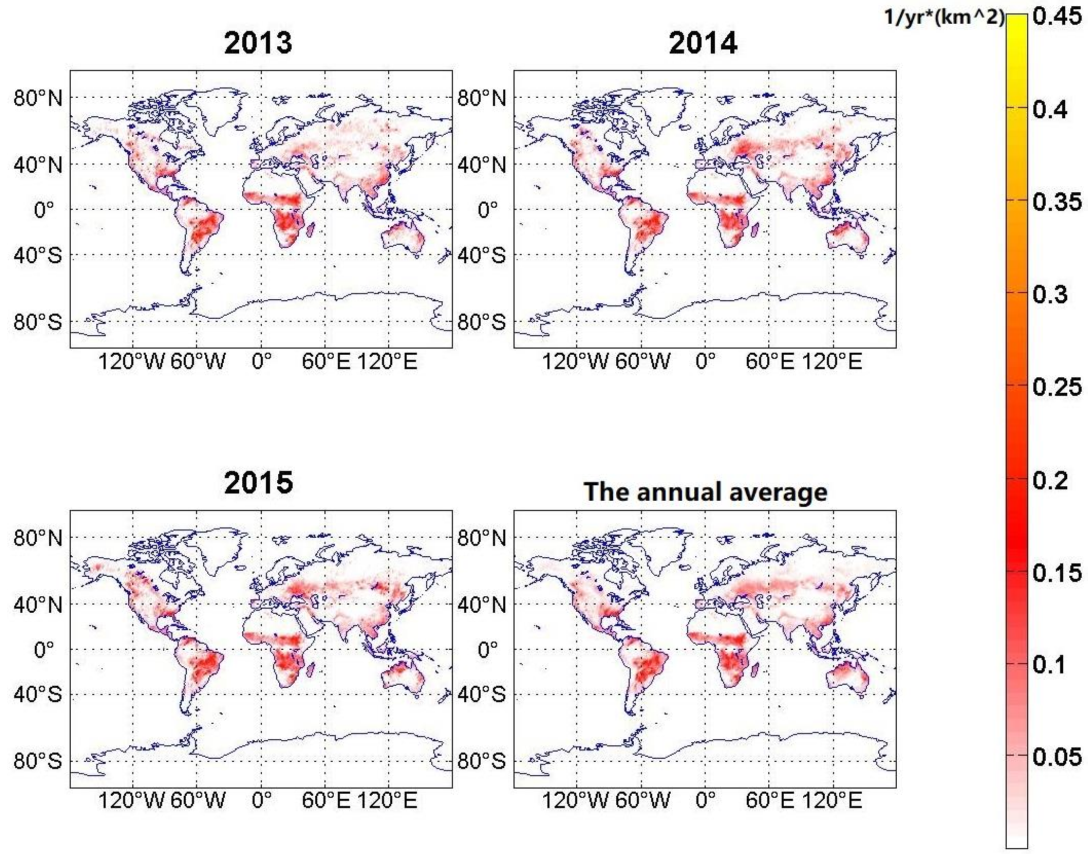

Fig.4 The spatial distribution of global fires from 2001 to 2015

3.1.3 Interannual variation of partial combustion zones of global wildfires

The GFEDv4 series of data divides the world into 14 sub-areas, namely BONA (Boreal North America), TENA (Temperate North America), CEAM (Central American), NHSA (Northern South America), SHSA (Southern Hemisphere South America), EURO (Europe), MID (Middle East), NHAF (Northern Hemisphere Africa), SHAF (Southern Hemisphere Africa), BOAS (Boreal Asia), CEAS (Central Asia), SEAS (Southern Asia), EQAS (Equatorial Asia), AUST (Australia and New Zealand) (Fig.5). According to the interannual variation of different regions of the global wildfires area, in most areas, especially in SHSA, NHAF, SHAF, CEAS, AUST, the wildfires have the largest burned area in 2002 and 2012, which is consistent with the maximum the wildfires area of global; in most areas of 2006, 2009, and 2013, the area of wildfires is relatively small, consistent with global results; the results of wildfires area and the number of wildfires are basically the same. In addition, SHSA (Southern Hemisphere South America), NHAF (Northern Hemisphere Africa), SHAF (Southern Hemisphere Africa), AUST (Australia and New Zealand) have a large wildfires area, which is highly consistent with the results obtained in Fig. 4. Besides, NHAF (Northern Africa), SHAF (Southern Africa), and SHSA (South America) are the main wildfires-affected areas, the total wildfires area from 2001 to 2015 is about 2148 million ha, accounting for nearly 80% of the global wildfires area in these 15 years. (Fig. 6). The results indicate that the wildfires area and the number of wildfires as two different reflections have high consistency.

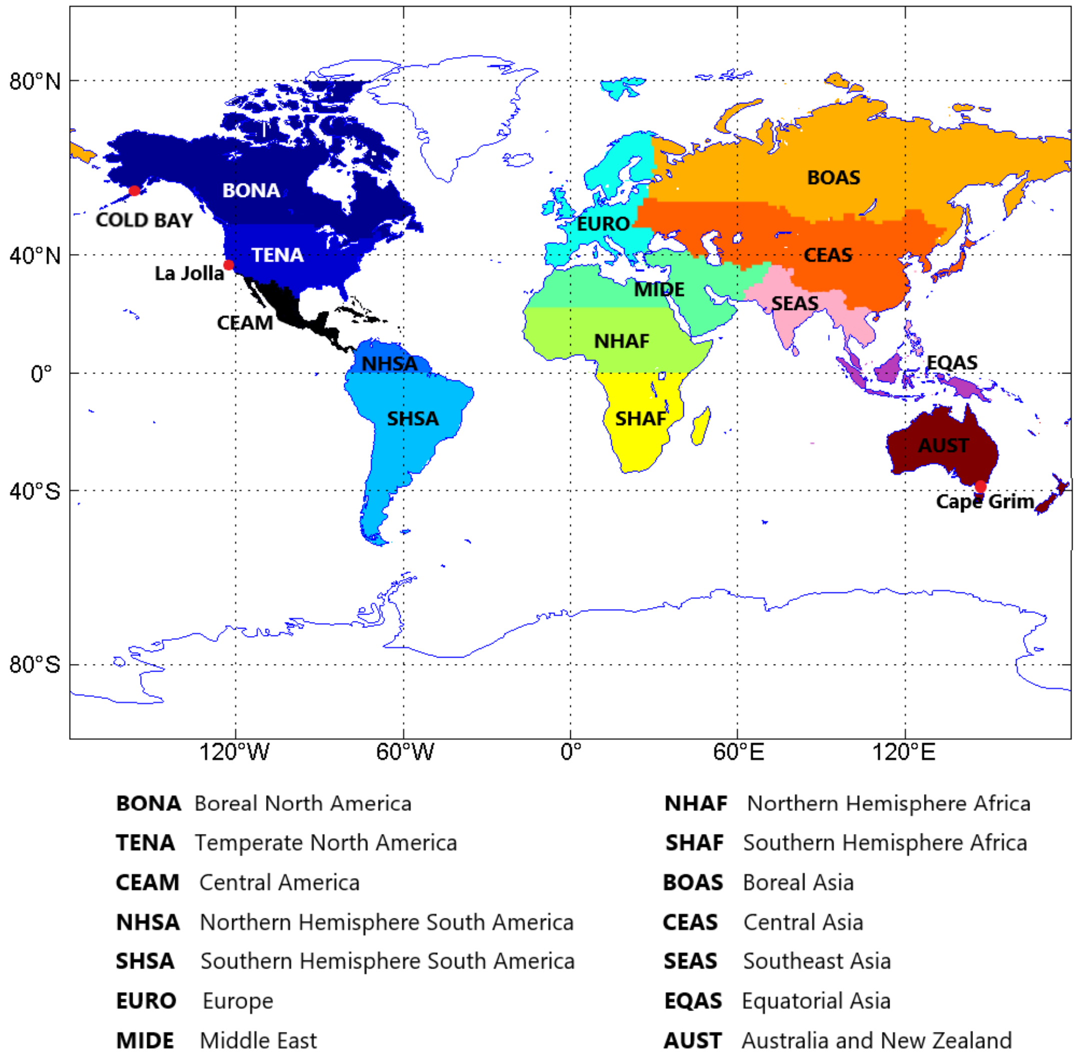

Fig.5 The 14 sub-areas of the GFEDv4 series

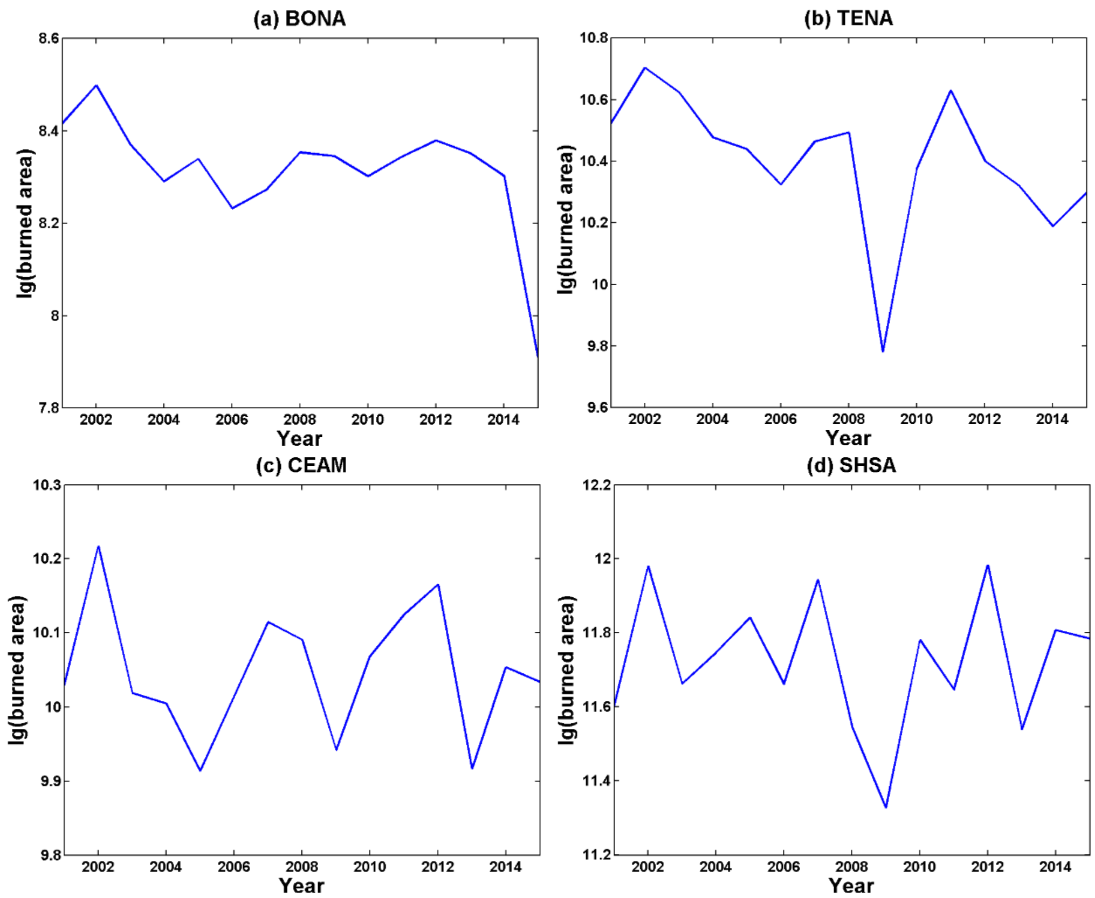

(a) BONA
(b) TENA
(c) CEAM
(d) SHSA
lg(burned area)
Year

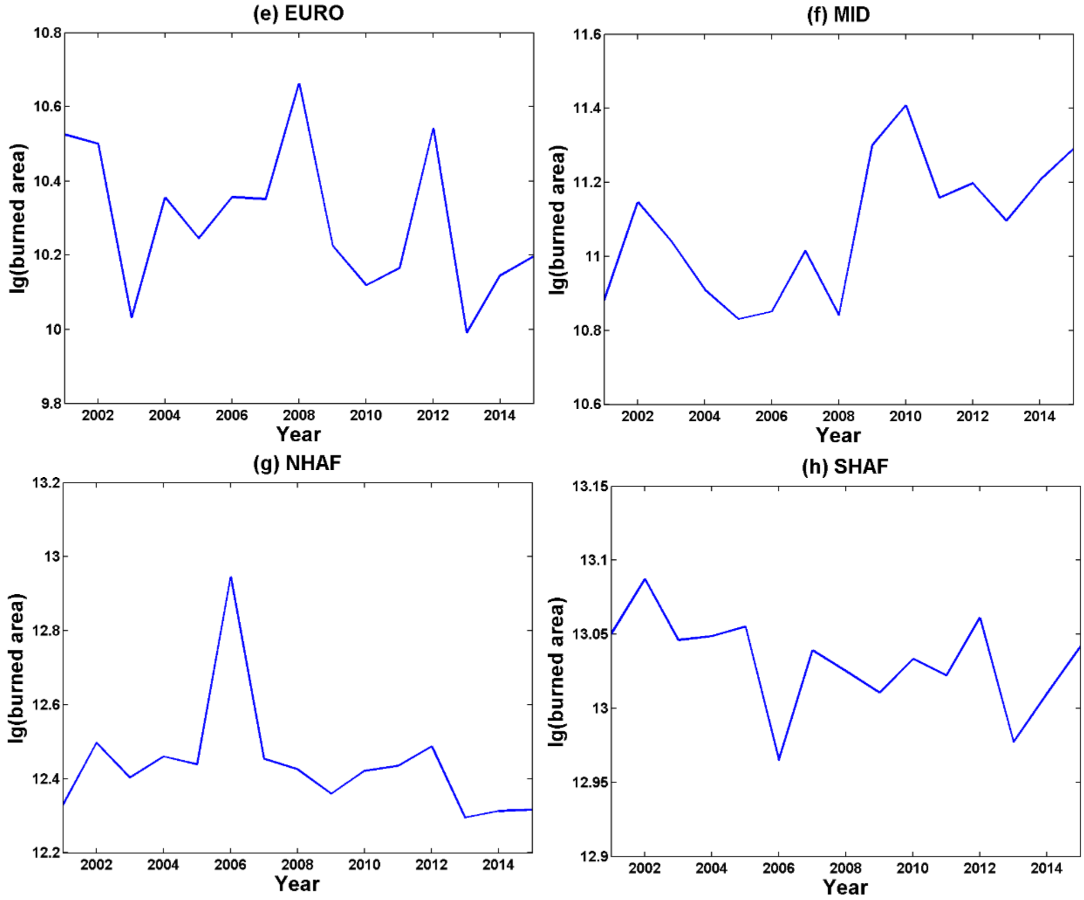

(e) EURO
(f) MID
(g) NHAF
(h) SHAF
lg(burned area)
Year

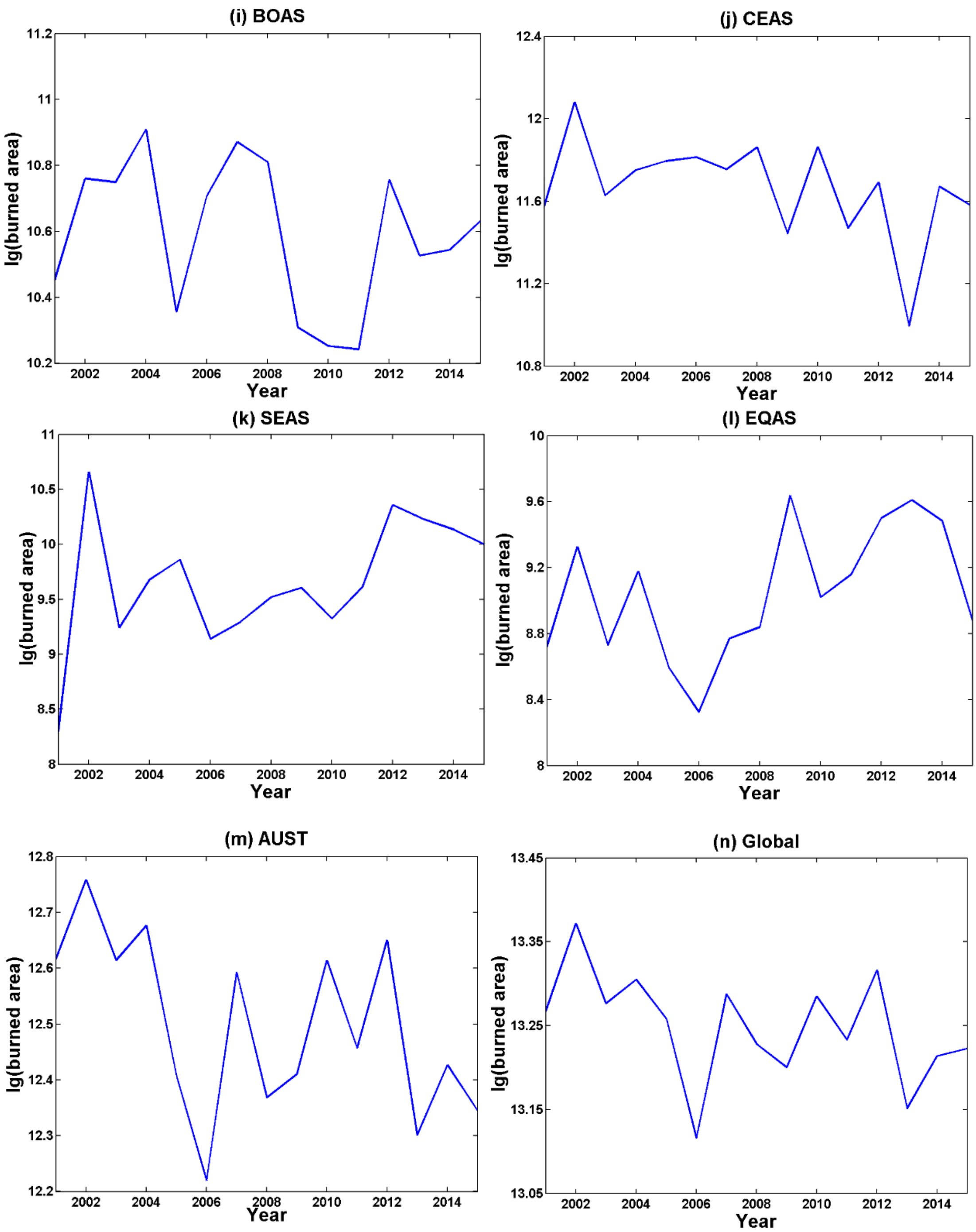

Fig.6 Interannual variation of different divisions of global wildfires area

3.2 Correlation analysis of wildfires and meteorological elements

3.2.1 Correlation analysis of global wildfires and meteorological elements

From Fig. 7(a)-7(d): Globally, the wildfires area is generally positively correlated with temperature, and the average of the global correlation coefficient $r_T = 0.47$. Except for a few regions in Eurasia and parts of Africa, the world is positively correlated; The wildfires area and wind speed are positively correlated in some regions, such as BONA and SHAF, and negatively correlated in a few regions, such as TENA and NHSA. The average of the global correlation coefficient $r_{wind} = 0.17$; The wildfires area and precipitation are generally negatively correlated. The average of the global correlation coefficient $r_{rain} = -0.41$, except for some areas of central

Africa, both are almost negatively correlated; The wildfires area is positively correlated with relative humidity in some areas, such as central South America, central Africa, and southern Africa. Most areas are negatively correlated, such as North America and Eurasia. The average global correlation coefficient $r_{RH} = -0.19$.

It can be seen that on a global scale, the wildfires area is generally positively correlated with temperature, generally negatively correlated with precipitation. And in many areas positively correlated with wind speed and negatively correlated with relative humidity.

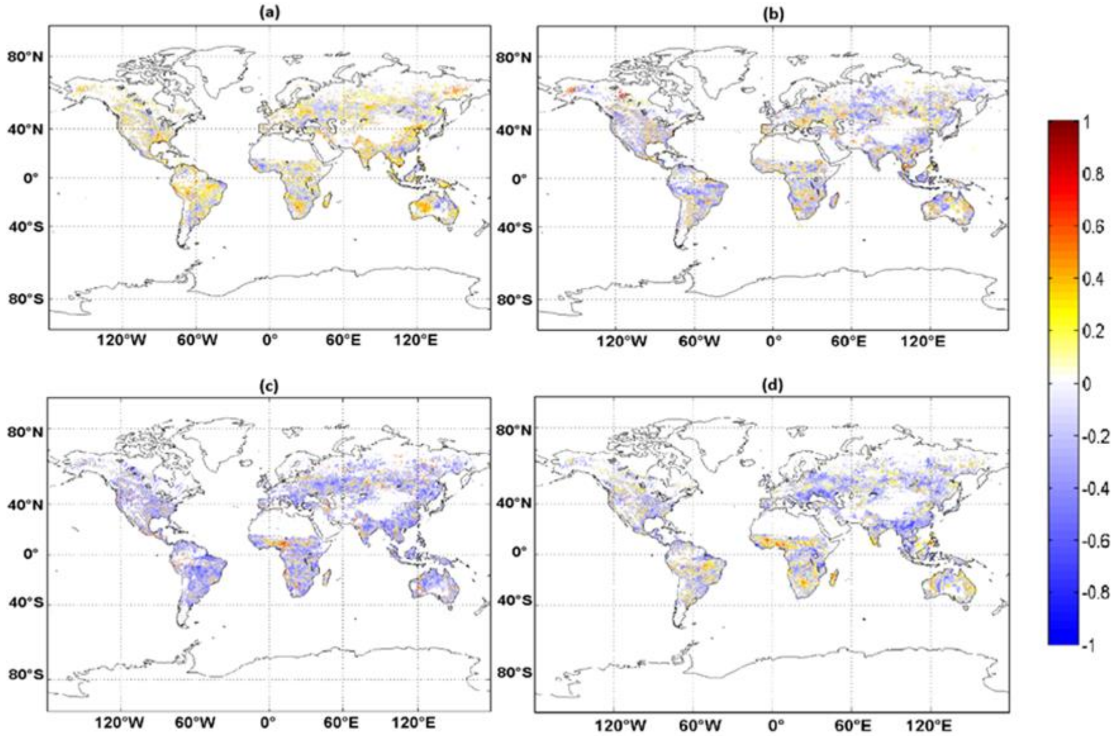

Fig. 7 Correlation between global wildfires area and meteorological elements

a for temperature, b for wind, c for precipitation, d for relative humidity

3.2.2 Correlation analysis of wildfires and meteorological elements in some areas

Considering that six of the nine observation stations for oxygen concentration are located on the ocean or in the polar regions, three regions with oxygen concentration observation stations on land were selected, namely the Boreal North America (BONA, COLD BAY), the Temperate North American (TENA, La Jolla), Australia (AUST, Cape Grim), to do the correlation analysis between wildfires and meteorological elements.

As shown in Fig. 9, the correlation coefficients obtained by NCEP/NCAR reanalysis data and ERA5 reanalysis data are basically the same. From Fig. 9(a)-9(d): In BONA, the temperature has a positive correlation with the forest burning area, except for 2005, 2006, and 2007; The precipitation is negatively correlated with the wildfires area, except for 2006 and 2010; Relative humidity is generally negatively correlated with the wildfires area, except for 2003 and 2009, but the correlation is weaker than the precipitation and temperature; The wind speed is positively correlated with the wildfires area, except for 2002, 2006 and 2009. From Fig. 8(a)-8(d): The change of wildfires area in most years is consistent with temperature; The wildfires area is basically opposite to the change of precipitation, but the interannual change of wildfires area has a certain downward trend, and the upward trend is not shown on the precipitation line; In most years, the relative humidity is opposite to the change in wildfires area; The change in wind speed is consistent with the change in wildfires area.

From Fig. 9(e)-9(h): In TENA, the temperature has a positive correlation with the wildfires area; There is a negative correlation between the precipitation and wildfires area; Relative humidity has a certain negative correlation with fire burning area, Except for 2004, 2009, and 2013. But the correlation is weaker than the precipitation and temperature; The wind speed is negatively correlated with the wildfires area in the TENA, but the correlation is weak. From Fig. 8(e)-8(h), the wildfires area in most years is consistent with changes in air temperature, which is basically opposite to precipitation, relative humidity, and wind speed.

From Fig. 9(i)-9(l): In AUST, the temperature has a positive correlation with the wildfires area, except for 2005, 2008, 2012, and 2013; The precipitation is negatively correlated with the wildfires area, except for 2005, 2010, and 2013; Relative humidity is negatively correlated with wildfires area, but the correlation is weaker than that of air temperature and precipitation; The correlation between wind speed and wildfires is difficult to draw.

In summary, the wildfires in different areas is related to various meteorological elements. In BONA, the wildfires area is positively correlated with air temperature and wind speed, negatively correlated with relative humidity and precipitation. In TENA, the wildfires area is positively correlated with air temperature, negatively correlated with wind speed, relative humidity, and precipitation. In AUST, the wildfires area is positively correlated with air temperature, negatively correlated with relative humidity and precipitation.

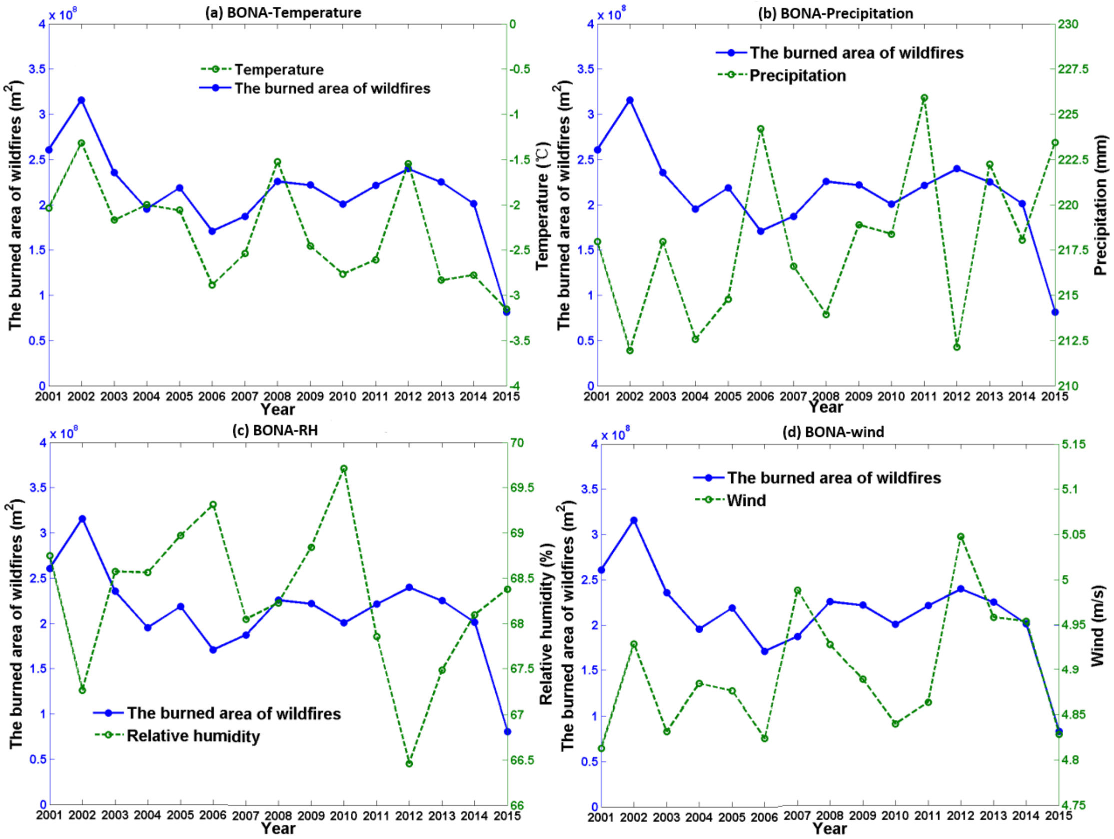

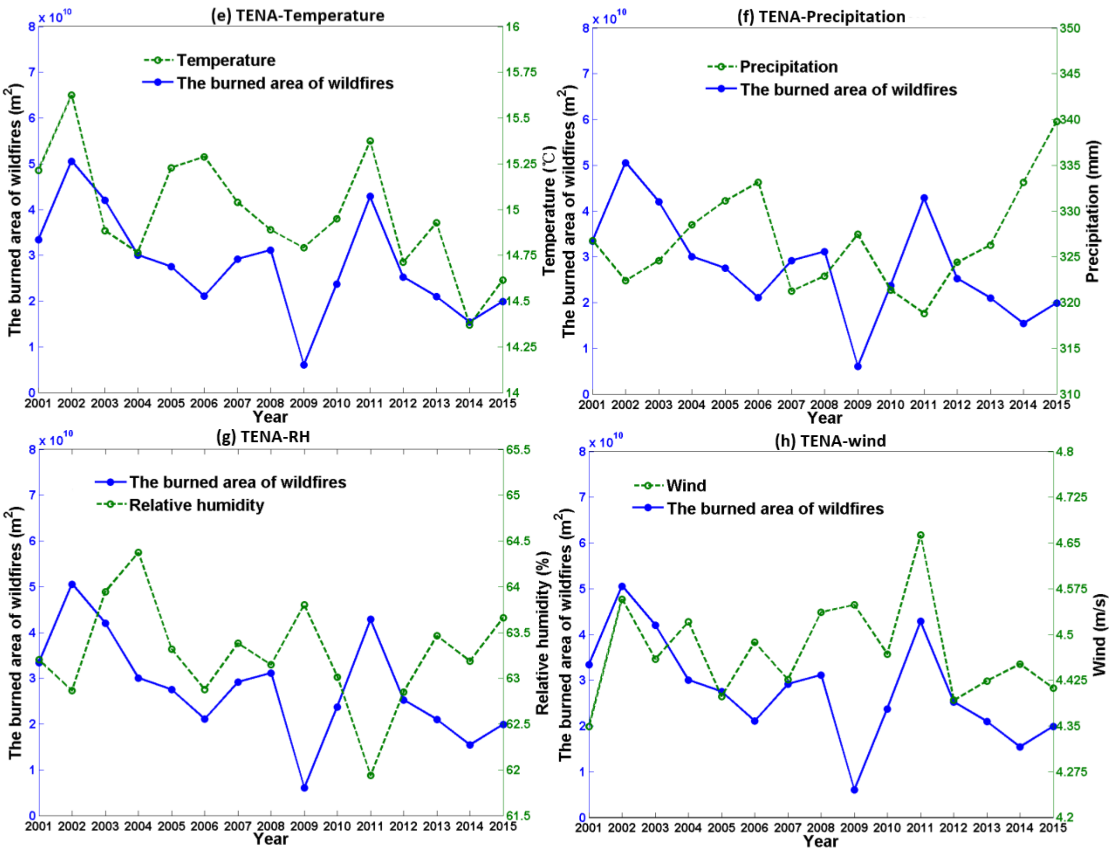

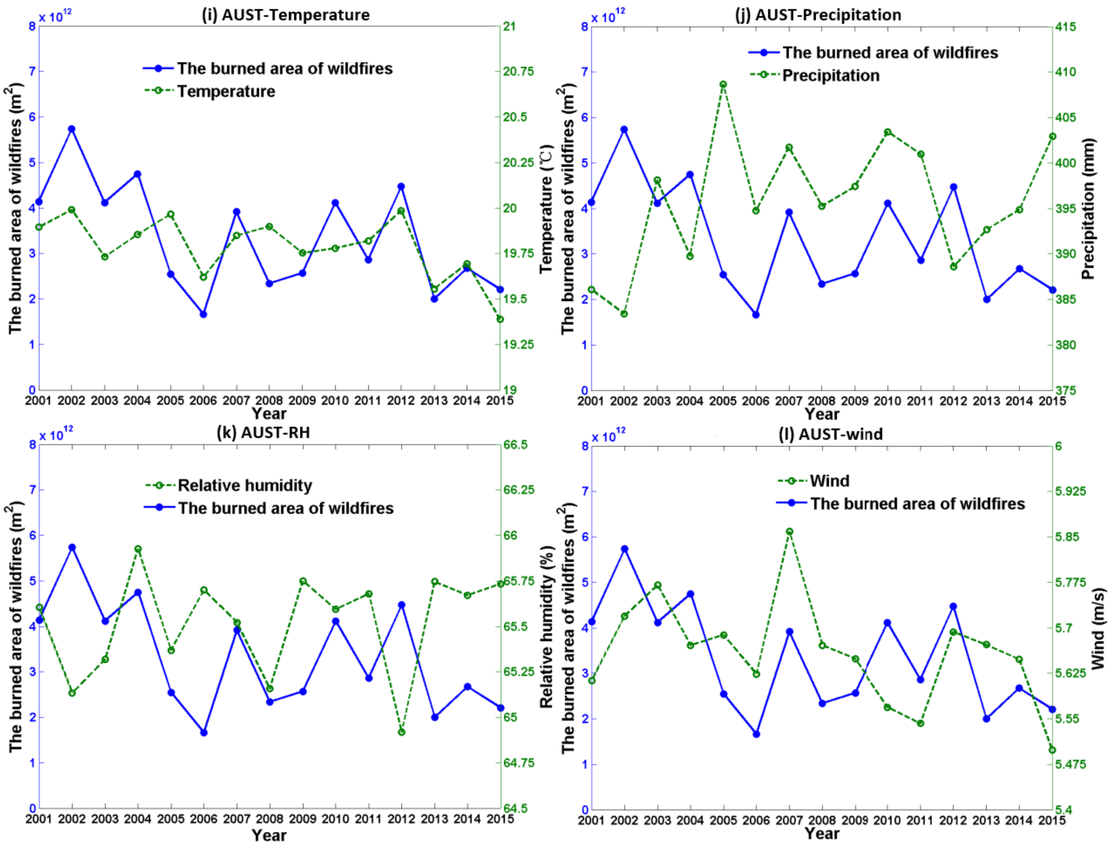

Fig.8 The annual variation of the wildfires area and meteorological elements in BONA, TENA and AUST

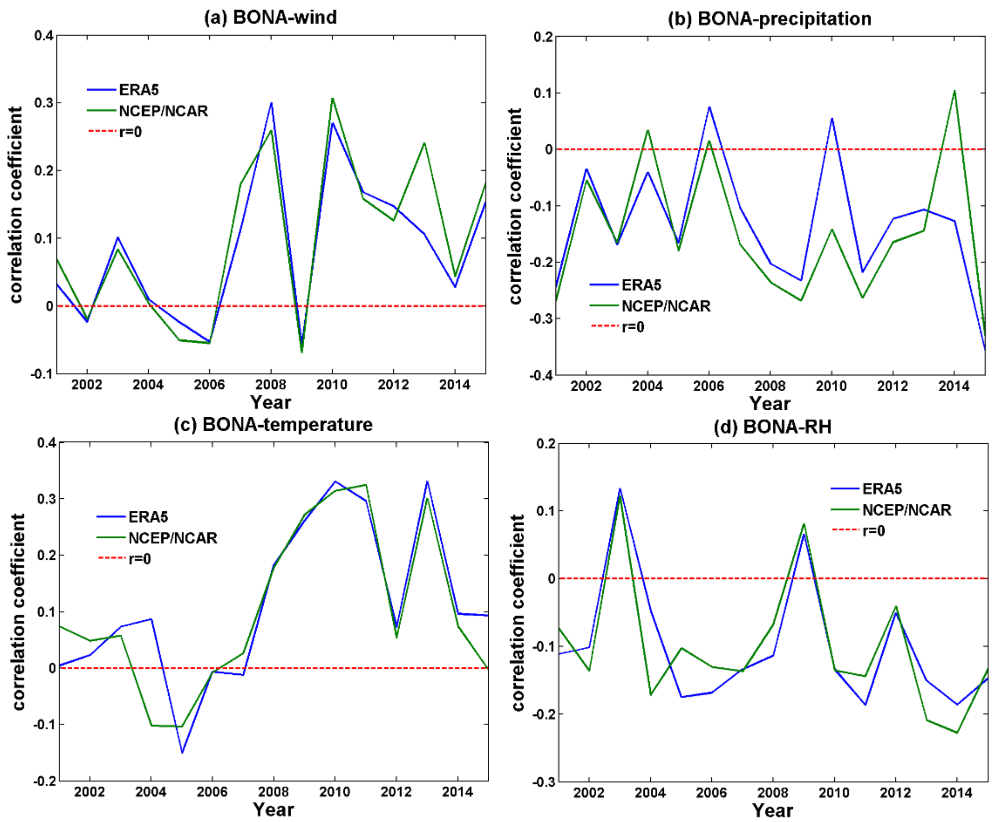
(a) BONA-wind
(b) BONA-precipitation
(c) BONA-temperature
(d) BONA-RH
ERA5
NCEP/NCAR
r=0
correlation coefficient
Year

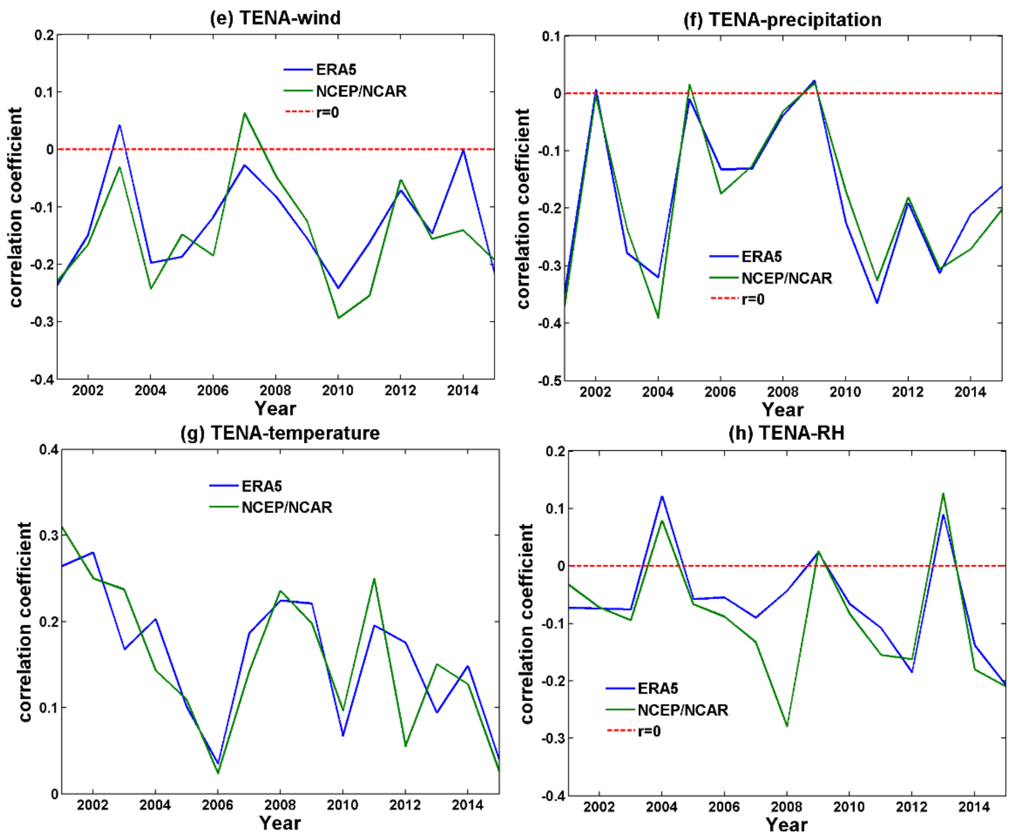
(e) TENA-wind
(f) TENA-precipitation
(g) TENA-temperature
(h) TENA-RH
ERA5
NCEP/NCAR
r=0
correlation coefficient
Year

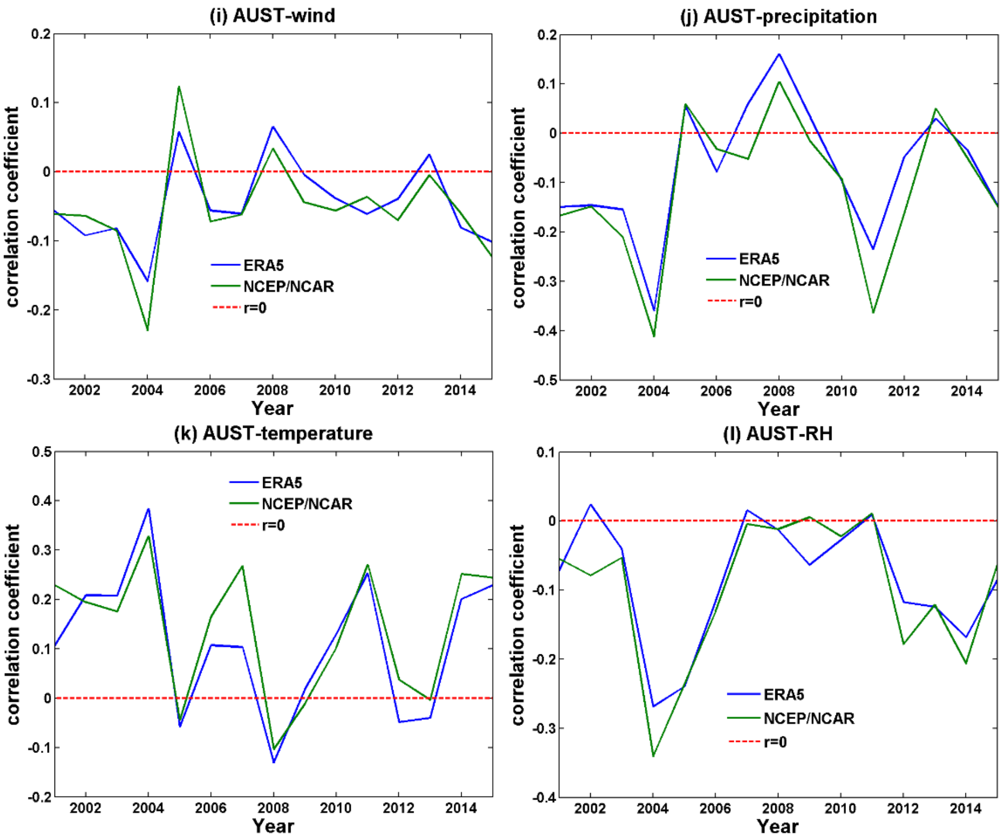

Fig. 9 The correlation between the wildfires area and the meteorological elements in BONA, TENA and AUST

3.3 Comprehensive analysis of meteorological elements and oxygen concentration in wildfires

3.3.1 Correlation between wildfires and oxygen concentration in some areas

Three areas BONA, TENA and AUST were selected for correlation analysis between wildfires area and oxygen concentration. From Fig. 11(a), except for 2005 and 2010, the oxygen concentration in the BONA has a positive correlation with the wildfires area; From Fig. 10(a), from 2001 to 2015, the correlation coefficient between oxygen concentration and wildfires area is $r_{O_2} = 0.61$. Meanwhile, the oxygen concentration showed a downward trend, and the wildfires area also showed a certain downward trend, but in some years, such as 2010, the two showed opposite changes. From Fig. 11(b), the oxygen concentration has a positive correlation with the wildfires area; From Fig. 10(b), the correlation coefficient is $r_{O_2} = 0.62$. The oxygen concentration showed a downward trend, the wildfires area also showed a certain downward trend, and the positive values of the wildfires area in 2002, 2007, and 2014 were also the corresponding extreme points of the oxygen concentration. From Fig. 11(c), except for 2009 and 2014, the oxygen concentration in AUST has a positive correlation with the wildfires area.; From Fig. 10(c), the correlation coefficient is $r_{O_2} = 0.60$. Meanwhile, the oxygen concentration showed a downward trend, the wildfires area also showed a certain downward trend in most years, and the positive values of the wildfires area in 2002, 2008, and 2010 were also the corresponding extreme points of the oxygen concentration.

Because air density is affected by altitude, the higher the altitude, the lower the air density, and therefore, the lower the oxygen concentration. The sea level pressure is also related to altitude. The higher the altitude, the lower the sea level pressure. Fig. 12 is the correlation of the global wildfires area and the sea level pressure. As can be seen from Fig. 12, on the global scale, the wildfires area is generally positively correlated with the sea level pressure, the average value of the global correlation coefficient $r_p = 0.38$, except for a few areas in Eurasia and parts of Africa, the wildfires area is basically positively correlated with the sea level pressure.

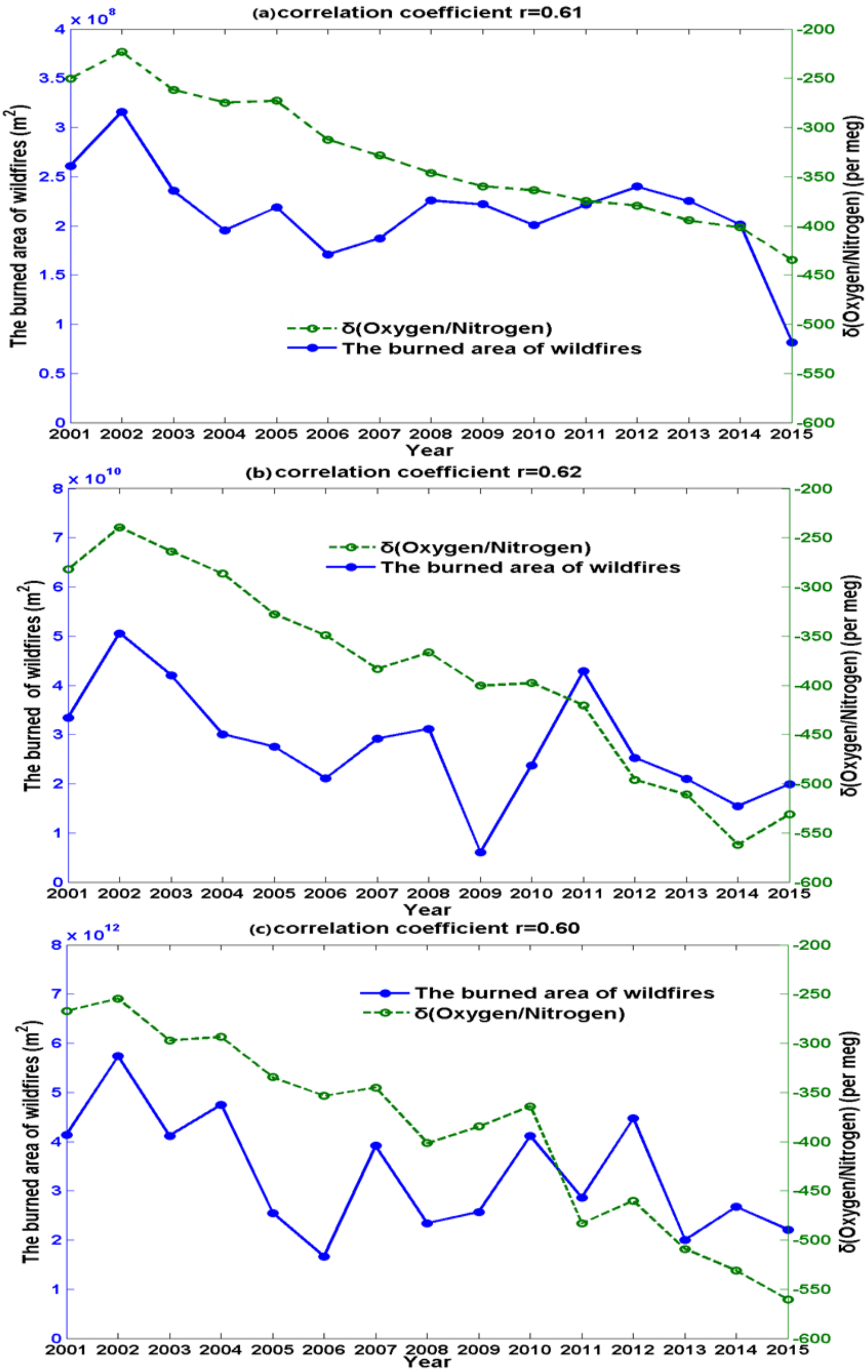

Fig. 10 The annual variation of the wildfires area and oxygen concentration in BONA, TENA and AUST

a for BONA, b for TENA, c for AUST

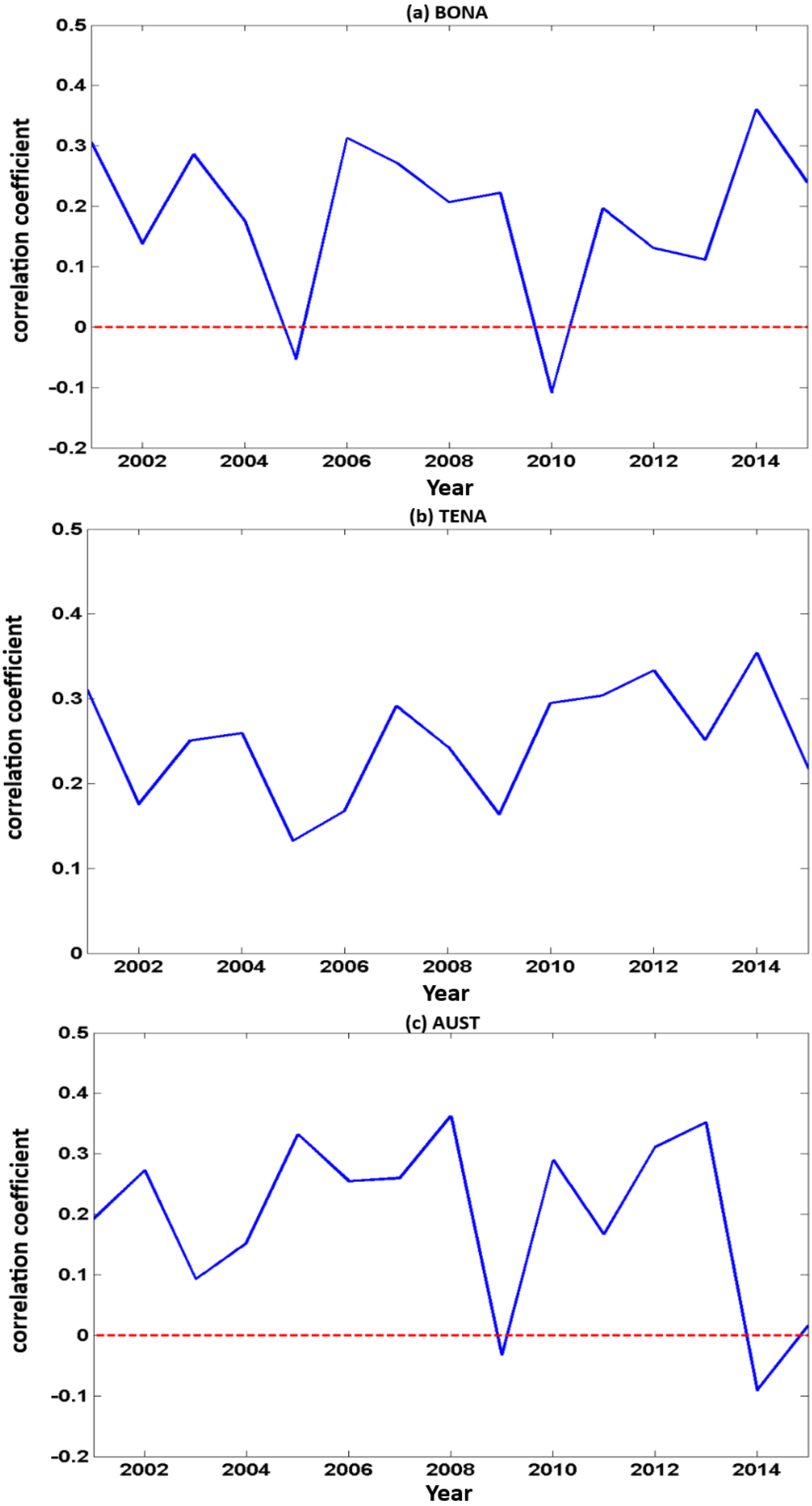

Fig. 11 The correlation between the wildfires area and the oxygen concentration in BONA, TENA and AUST

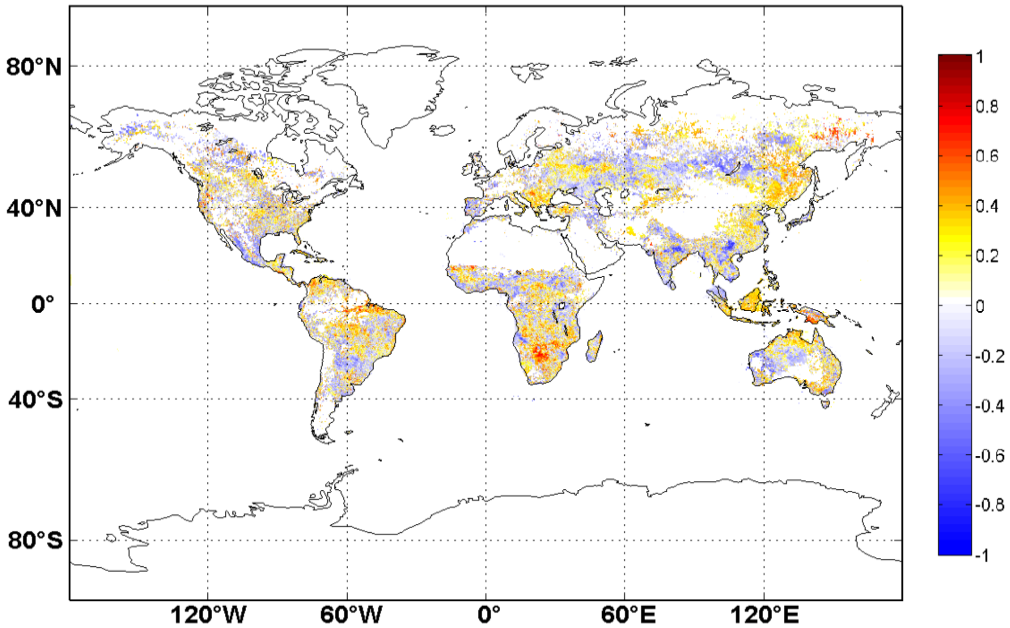

Fig. 12 Correlation between global wildfires area and sea level pressure

3.3.2 Comprehensive analysis of meteorological elements and oxygen concentration in wildfires

In the Boreal North America (BONA), the Temperate North America (TENA), the Australia and New Zealand (AUST), the effects of five factors on the wildfires area are as follows: oxygen> temperature> precipitation> wind> relative humidity. Relative to the simple correlation coefficient, the direct path coefficients of oxygen and wind are relatively large, indicating that the impact of the two on the wildfires area mainly comes from its own role. The direct path coefficients of precipitation and relative humidity on the wildfires area are small, indicating that precipitation and relative humidity affect wildfires mainly by using other factors such as temperature. According to the calculation, the remaining path coefficients $p_{ye1} = 0.52$, $p_{ye2} = 0.61$, $p_{ye3} = 0.55$, the values are relatively large, indicating that there are still other factors (such as the terrain and the types of forests) that have a great impact on the wildfires area (Table 3).

Table3 The direct path coefficients of different meteorological elements in BONA, TENA, AUST

area	**the direct path coefficients of different elements**				
	Temperature	Precipitation	Relative humidity	Wind	Oxygen concentration
BONA	0.36	-0.26	-0.13	0.22	0.38
TENA	0.34	-0.21	-0.08	0.18	0.37
AUST	0.35	-0.23	-0.17	0.2	0.39

4 Discussion and conclusion

4.1 Discussion

In the analysis of the correlation between global wildfires and meteorological elements, some studies have shown that (Qin, 2005) wildfire risks are determined by the state of combustibles and the comprehensive background in which they are located. A very important part of comprehensive background is the meteorological factors (temperature, relative humidity, precipitation, wind speed, etc.). Qin (2005) define an index of the impact of meteorological elements on wildfires, which named $\mathrm{F(WI)}$. The index $\mathrm{F(WI)}$ can be expressed as:

$$\mathrm{F(WI)} = \mathrm{F(T, H, P, S)}$$

Where T, H, R, S represent temperature, relative humidity, precipitation, wind speed, respectively.

In terms of the correlation between wildfires and wind, some studies have found that (Jia et al., 1987) general wildfires have a small fire area, short duration, and limited wind field impact; however, the mega-wildfires will form a small-scale weather system (a new low-pressure system) with its own temperature and pressure field configuration, which has a significant influence on the spread and attenuation of the wildfires. Studies have shown that (Grenier et al., 2005; Li et al., 2009) precipitation anomalies are one of the easiest ways to measure the anomaly of precipitation in a region. For wildfires and precipitation, precipitation will directly affect the water content of combustibles in the forest area. The more humid the surface, the higher the water content of the vegetation, the lower probability of wildfires, so the precipitation anomaly has a correlation with the occurrence of wildfires. For wildfires and air humidity, air humidity has a certain influence on the water content of combustibles. However, because the relative humidity is determined by meteorological factors such as temperature and air moisture content, air humidity has an impact on wildfires but limited. For wildfires and temperature, the increase in temperature will cause the relative humidity to decrease, and the increase in temperature can reduce the water content of the combustibles, and bring the surface temperature of the combustibles closer to the point of ignition.

The burning of forests must have three conditions: combustible, combustion-supporting, and ignition (Li et al., 2009). Studies indicate that (Hamins, 2003; Laurent et al., 2013) for the fire model modeling, consider its own elements such as HGL temperature (hot flue gas layer temperature), HGL thickness (hot flue gas layer thickness), top jet temperature, fire plume temperature, flame height, oxygen concentration, smoke concentration, heat radiation flux, etc. Changing the oxygen concentration by 1% can change the results of the fire model by 8%-9%. Oxygen consumption during combustion is proportional to the rate of combustion. The following formula is used to describe the relationship between the oxygen consumption Y_i and the initial oxygen concentration y_i during combustion:

$$Y_i = \frac{y_i \dot{m}}{\dot{m}_e} = \frac{y_i \dot{Q}}{\chi_a H_c \dot{m}_e}$$

$\dot{m} = \dot{Q}/\chi_a H_c$, $\dot{m}$ is the fuel mass burn rate, $\dot{Q}$ is the heat release rate, H_c is the flame height, χ_a is the burning index, and $\dot{m}_e$ is the oxygen mass rate entering the hot flue gas layer.

Since oxygen directly affects the wildfire by affecting the combustion process, the change in oxygen concentration has a great impact on the occurrence of wildfires, and the two have a high correlation. Paleoclimate studies have shown (Abdallah et al., 2012) that fossil charcoal, inertinites, and the pyrogenic polycyclic aromatic hydrocarbons (PAHs) are the only direct evidence of the occurrence of ancient wildfires. These evidences indicate that the frequency of wildfires in the early Triassic period has dropped significantly, and this is related to a significant drop in atmospheric oxygen concentrations after or during the end of the Permian mass extinction event. Scholars (Belcher et al., 2010b; Berner,2009) generally believe that the decline in oxygen concentration is the main reason for the low number of wildfires during that period. This also confirms that the oxygen concentration has a very important impact on the occurrence of wildfires.

The current trend of decreasing O_2 concentration in the atmosphere is significant. Population growth, fossil fuel combustion, deforestation, and dry land expansion further exacerbate the decline in global oxygen concentrations (Huang et al., 2018; Keeling, 1988). In addition, in the context of global warming, the contribution of temperature is getting sincerely important. However, the global meteorological factors and oxygen concentration changes are complex. Therefore, the next step is to improve the wildfire models, analyze the contribution of different factors to wildfires occurrence, and then estimate future wildfires in the context of global warming.

4.2 Conclusion

This study used MOD14A2 data, NCEP/NCAR reanalysis data set Ⅰ, ERA5 reanalysis data, GFEDv4 data and the Scripps O_2 data, using the correlation analysis and path analysis to analyze the correlation between wildfires, meteorological elements and oxygen concentration in BONA, TENA and AUST. The following preliminary results were obtained:

1) Global wildfires occurred more frequently in 2002 and 2012, with severe wildfires disasters in the South America, Northern Africa, and Southern Africa. These areas accounted for nearly 80% of the global wildfires area from 2001 to 2015.

2) Different meteorological elements have very different effects on the occurrence of wildfires. Globally, the correlation coefficient between temperature and wildfires area is 0.47, between wind speed and wildfires area is 0.17, between precipitation and wildfires area is -0.41; between relative humidity and wildfires area is -0.19.

3) Oxygen concentration can be regarded as a variable independent of meteorological elements. In BONA, from 2001 to 2015, the correlation coefficient between oxygen concentration and wildfires area is 0.61; In TENA, the correlation coefficient is 0.62; In AUST, the correlation coefficient is 0.6.

Acknowledgements

This work was jointly supported by the National Natural Science Foundation of China (4167501 7), the Ministry of Science and Technology of the People's Republic of China (2018YFB1502800) and the autonomous project "Study on the Relationship between Atmospheric Oxygen Concentra tion and Forest Fire" of the Key Laboratory of Land Surface Process and Climate Change in Cold a nd Arid Regions of Chinese Academy of Sciences. The authors acknowledge NASA, USA for providi ng the wildfires data(MOD14A2 and GFEDv4), the Scripps Institution of Oceanography, USA for at mospheric O2 levels data, NCEP/NCAR, USA for the data of NCEP/NCAR Reanalysis I, European Ce ntre for Medium-Range Weather Forecasts (ECMWF) for the ERA5 Reanalysis data.

Data Availability Statement

The global fire data comes from MOD14A2 data (https://modis-land.gsfc.nasa.gov/fire.html); Global wildfires area data comes from GFEDv4 (Global Fire Emissions Database, Version 4.1), provided by NASA (https://daac.ornl.gov/VEGETATION/guides/fire_emissions_v4_R1.html). The meteorological data come from ERA5 data provided by ECMWF (https://cds.climate.copernicus.eu/cdsapp#!/dataset/reanalysis-era5-pressure-levels-monthly-m eans?tab=overview) and NCEP/NCAR reanalysis data set I produced by NCEP and NCAR (https://www.esrl.noaa.gov/psd/data/gridded/reanalysis/#opennewwindow). The observational O_2 concentration data comes from the Scripps O_2 program (http://scrippso2.ucsd.edu/).

References

1. Abdallah, M., Hamad, A.-J., Dieter U. (2012). The record of Triassic charcoal and other evidence for palaeo-wildfires: Signal for atmospheric oxygen level, taphonomic biases or lack of fuel. International Journal of Coal Geology 96, 60-71.
2. Anderson, K.R., Englefield, P., Little, J., & Reuter, G. (2009). An approach to operational forest fire growth predictions for Canada. International Journal of Wildland Fire 18, 893-905. DOI: 10.1071/WF08046
3. Andrews, P.L. (2014). Current status and future needs of the BehavePlus fire modeling system. International Journal of Wildland Fire 23, 21-33. DOI: 10.1071/WF12167
4. Balbi, J.H., Morandini, F., Silvani, X., Filippi, J.B., & Rinieri, F. (2009). Physical model for wildland fires. Combust. Flame 156, 2217-2230. DOI: 10.1016/j.combustflame.2009.07.010.
5. Belcher, C.M., Yearsley, J.M., McElwain, J.C., & Rein,G. (2010b). Baseline intrinsic flammability of Earth's ecosystem estimated from paleoatmospheric oxygen over the past 350 million years. Proceedings of the National Academy of Sciences of United States of America, 107: 22448-22453. DOI: 10.1073/pnas.1011974107
6. Berner, R.A. (2009). Phanerozoic atmospheric oxygen: new results using the GEOCARBSULF model. American Journal of Science, 309: 603–606. DOI: 10.2475/07.2009.03.
7. Bowman, D. M. J. S., Balch, J.K., Artaxo, P., Bond, W.J., Carison, J.M., et al., (2009). Fire in the Earth system. Science 324, 481–484. https://science.sciencemag.org/content/324/5926/481
8. Bradshaw, L.S., Deeming, J.E., & Burgan, R.E. (1983). The 1978 NFDRS: technical documentation. USDA Forest Service, Report No. Gen Tech Rep INT-169, 44 (U.S. Department of Agriculture, Forest Service, Intermountain Forest and Range Experiment Station, Missoula, MT, USA).
9. Chen, Y., Randerson, T., Douglas C.M., DeFries, R.S., Collatz, G.J., et al. (2011). Forecasting Fire Season Severity in South America Using Sea Surface Temperature Anomalies. Science 334, 787-791. DOI: 10.1126/science.1209472.
10. Chen, Y., James T.R., & Douglas C.M. (2015). Tropical North Atlantic ocean-atmosphere interactions synchronize forest carbon losses from hurricanes and Amazon fires. Geophysical Research Letters 42, 6462-6470. DOI: 10.1002/2015GL064505
11. Chen, Y., Douglas, C.M, Niels, A., Giglio, L., Randerson, J.T., et al. (2016). How much global burned area can be forecast on seasonal time scales using sea surface temperatures? Environmental Research Letters 11, 1-13. DOI: 10.1088/1748-9326/11/4/045001
12. Chen, Y., Morton, D.C., Andela, N., van der Werf, G.R., Giglio, L., et al. (2017). A pan-tropical cascade of fire driven by El Niño/Southern Oscillation. Nature Climate Change 7, 906-911. DOI: 10.1038/s41558-017-0014-8.
13. Cruz, G.M. (2010). Monte carlo-based ensemble method for prediction of grassland fire spread. International Journal of Wildland Fire 19, 521-530. DOI: 10.1071/WF08195.
14. Di, L.Y., Sun, R.Y. (2007). Summarization of research on Forest Fire in China. Journal of Catastrophology 22, 118-123. DOI: 1000-811X(2007)22:4<118:ZGSLHZ>2.0.TX;2-8.

15. Ding, Q., & Feng, X.F. (2013). Change analysis of boreal forest fire using MODIS thermal anomalies product for European Russia. Journal of Geo-Information Science 15, 476-482. DOI: 1560-8999(2013)15:3<476:OYBFSL>2.0.TX;2-W.
16. Finney, M.A. (1998). FARSITE: Fire Area Simulator-Model Development and Evaluation. Rocky Mountain Research Station Research Paper. RMRS-RP-4. USDA Forest Service, Missoula: pp, 52.
17. Finney, M.A. (2002). Fire growth using minimum travel time methods. Canadian Journal Forest Research 32, 1420-1424. DOI: 10.1139/X02-068
18. Finney, M.A. (2006). An overview of FlamMap fire modeling capabilities. In: Proceedings RMRS-P-41. U.S. Department of Agriculture, Forest Service, Rocky Mountain Research Station, Fort Collins, CO, pp, 213-220.
19. Fu, L.L., Deng, Q.Z., & Weng, Y.J. (2014). The Transmission of international crude oil price fluctuation to domestic prices of agricultural product based on path analysis. Resources Science 36, 1418-1424. DOI: 1007-7588(2014)36:7<1418:GJYYJG>2.0.TX;2-Z.
20. Giglio, L., Csiszar, I., & Justice, C.O. (2006). Global Distribution and Seasonality of Active Fires as Observed with the Terra and Aqua MODIS Sensors. Journal of Geophysical Research: Biogeosciences, Vol. 111, G02016, doi:10.1029/2005JG000142.
21. Giglio, L., Randerson, J. T., van der Werf, G. R. (2013). Analysis of daily, monthly, and annual burned area using the fourth generation global fire emissions database (GFED4). Journal of Geophysical Research-Biogeosciences. 118, 317–328. https://agupubs.onlinelibrary.wiley.com/doi/pdfdirect/10.1002/jgrg.20042.
22. Grenier, D.J., Bergeron, & Y., Kneeshaw D. (2005). Firefrequency for the transitional mixed wood forest of Timiskaming, Quebec, Canada. Canadian Journal of forest research 35, 655-656.
23. Hamins, A. (2003). Report of Experimental Results for the International Fire Model Benchmarking and Validation Exercise #3.
24. Huang, J.P., Huang, J.P., Liu, X.Y., Li, C.Y., Ding, L., et al. (2018). The global oxygen budget and its future projection. Science Bulletin 68, 1180-1186. DOI: 10.1016/j.scib.2018.07.023.
25. Intergovernmental Panel on Climate Change (IPCC). (2007). Climate change 2007: The Physical Science Basis. (Cambridge Univ. Press).
26. Jia, S.Q., Jia, L., & Ende J. (1987). On the temperature and pressure wind field in the mega forest fire zone. Journal of Northeast Forestry University 15, 226-232.
27. Keeling, R.F. (1988). Measuring correlations between atmospheric oxygen and carbon dioxide mole fractions - a preliminary-study in urban air. Journal of Atmospheric Chemistry 7, 153–176. DOI: 10.1007/BF00048044.
28. Lassus, J., Courty, J., Garo, J.P., Studer, E., Jourda, P., et al. (2014). Ventilation effects in confined and mechanically ventilated fires. International Journal of Thermal Sciences 75, 87-94. DOI: 10.1016/j.ijthermalsci.2013.07.015.
29. Laurent, G., Bertrand, S., Fatiha, N. (2013). MAGIC and Code_Saturne developments and simulations for mechanically ventilated compartment fires. Fire Safety Journal 62, 161-173.
30. Li, H.G., Mei, X., & Xiao, W.M. (2009). The close relation of forest fire disaster and meteorology factors. Forest Investigation Design 152, 109-110.
31. Li, X.L. (2016). Synergy of multi-factors for forest fire prediction and detection based on MODIS data. A dissertation for doctor's degree. (University of Science and Technology of

China, China).

32. Marlier, M.E., DeFries, R.S., Voulgarakis, A., Kinney, P.L., Randerson, J.T., et al. (2013). El Niño and health risks from landscape fire emissions in Southeast Asia. Nature Climate Change, 3: 131-136. https://www.nature.com/articles/nclimate1658.
33. Martin, M.V., Honrath, R.E., Owen, R.C., & Lapina, K. (2008). Large-scale impacts of anthropogenic pollution and boreal wildfires on the nitrogen oxides over the central North Atlantic region. Journal of Geophysical Research: Atmosphere, Vol. 111, D17308. DOI:10.1029/2007JD009689.
34. Matt J., Cochrane, M.A., Freeborn, P.H., Holden, Z.A., Brown, T.J., et al. (2014). Climate-induced variations in global wildfire danger from 1979 to 2013. Nature Communications 6, 1-11. DOI: 10.1038/ncomms8537
35. Monedero, S., Ramirez, J., Molina, T., & Cardil, A. (2017). Simulating wildfires backwards in time from the final fire perimeter inpoint-functional fire models. International Journal of Wildland Fire 92, 163-168. DOI: 10.1016/j.envsoft.2017.02.023.
36. Noble, I.R., Gill, A.M., & Bary, G.A. (1980). McArthur's fire-danger meters expressed as equations. Australian Journal of Ecology. 5, 201–203. DOI: 10.1111/j.1442-9993.1980.tb01243.x
37. Paulo, M. F., Ana M.G., Barros, A.P., Joao, A.S. (2016). Characteristics and controls of extremely large wildfires in the western Mediterranean Basin. Journal of Geophysical Research: Biogeosciences, Vol. 121. DOI: 10.1002/2016JG003389.
38. Pimont, F., Parsons, R., Rigolot, E., de Coligny, F., Dupuy, J.L., et al. (2016). Modeling fuels and fire effects in 3D: model description and applications. Environmental Modelling and Software 80, 225-244. DOI: 10.1016/j.envsoft.2016.03.003.
39. Potapov, P., Hansen, M.C., & Stehman, S.V. (2008). Combining MODIS and Landsat imagery to estimate and map boreal forest cover loss. Remote Sensing of Environment 112, 3708-3719. DOI: 10.1016/j.rse.2008.05.006.
40. Qin, X.L. (2005). Study on forest fire early warning and monitoring methodology using Remote Sensing and Geography Information System Techniques. A dissertation for doctor's degree. (Chinese Academy of Forestry, China)
41. Ramirez, J., & Monedero, S. (2011). Wildfire Analyst User's Guide: The Different Simulation Modes.
42. Rowekamp, M., Dreisbach, J., & Kelin, H. (2008). International Collaborative Fire Modeling Project (ICFMP), Summary of Benchmark Exercises. Report 227, GRS.
43. Sahanavin, N., Prueksasit, T., & Tantrakarnapa, K. (2018). Relationship between PM10 and PM2.5 levels in high-traffic area determined using path analysis and linear regression. Journal of Environmental Sciences 69, 105-114. DOI: 10.1016/j.jes.2017.01.017.
44. Sander, V., Rogers, B.M., Goulden, M.L., Jandt, R.R., Miller, C.E., et al., (2017). Lightning as a major driver of recent large fire years in North American boreal forests. Nature Climate Change 7, 529-536. DOI: 10.1038/NCLIMATE3329.
45. Schenk, K., Drossel, B., Schwabl, F. (2002). Self-organized critical forest-fire model on large scales. Physical Review 65, 026135. https://journals.aps.org/pre/abstract/10.1103/PhysRevE.65.026135.
46. Scott, J.H. (1999). NEXUS: a system for assessing crown fire hazard. Fire Manage 59, 21-24.
47. Shu, L.F., Zhang, X.L., Dai, X.A. (2003). Forest fire research(Ⅱ): Fire Forest. World Forestry

Research 136, 34-37. DOI: 1001-4241(2003)16:4<34:LHYJZS>2.0.TX;2-I.

48. Siegert, F., Ruecker, G., Hinrichs, A., & Hoffmann, A.A. (2001). Increased damage from fires in logged forests during droughts caused by El Nino. Nature 414, 437-440. DOI: 10.1038/35106547.
49. Stefan, W., Jeremy, R.S., Andrew, C., & Yates, C. (2013). Sensitivity of the MODIS fire detection algorithm (MOD14) in the savanna region of the Northern Territory, Australia. ISPRS Journal of Photogrammetry and Remote Sensing 76, 11-16. DOI: 10.1016/j.isprsjprs.2012.11.005.
50. Van Wagner, C. E. (1987). Development and structure of the Canadian forest fire weather index system. Report No. 1992 (Canadian Forestry Service, Petawawa National Forestry Institute, Chalk River, ON, Canada).
51. Wu, J.Y., Timithy, W.S., Janette, R.T., Kolka, R.K., & Franz, K.J. (2015). Watershed features and stream water quality: gaining insight through path analysis in a Midwest urban landscape,U.S.A. Landsc. Urban Plan 143, 219–229. DOI: 10.1016/j.landurbplan.2015.08.001.
52. Zhu, P., Wang, Z.-W., Qin, Z.-W., & Shen, Y. (2018). The transfer path analysis method on the use of artificial excitation: Numerical and experimental studies. Applied Acoustics 136: 102-112. DOI: 10.1016/j.apacoust.2018.02.007.